Master's thesis

NTNU
Norwegian University of Science and Technology
Faculty of Engineering
Department of Civil and Environmental Engineering

Mihail Boescu

Local soil classification and assessment of the mechanical properties with emphasis on pile adfreeze bond strength in Longyearbyen, Svalbard

Master's thesis in Cold Climate Engineering
Supervisor: Gustav Grimstad (NTNU), Thomas Ingeman-Nielsen (DTU), Aleksey Shestov (UNIS)
July 2022

NTNU
Norwegian University of Science and Technology

UNIS
The University Centre in Svalbard

DTU

Mihail Boescu

Local soil classification and assessment of the mechanical properties with emphasis on pile adfreeze bond strength in Longyearbyen, Svalbard

Master's thesis in Cold Climate Engineering
Supervisor: Gustav Grimstad (NTNU), Thomas Ingeman-Nielsen (DTU), Aleksey Shestov (UNIS)
July 2022

Norwegian University of Science and Technology
Faculty of Engineering
Department of Civil and Environmental Engineering

NTNU
Norwegian University of
Science and Technology

Abstract

Construction engineering practices have been a highly sensitive topic regarding the Arctic infrastructure. The limitations of the permafrost behavior impose an analysis from the thermal and mechanical point of view. The positive change in temperature is definitely increasing the active layer thickness, as well as the frost penetration depth during the seasonal variation of the temperature. During the past recorded years, the global climate change made the soil and infrastructure built on it more fragile and more susceptible to the warming of the climate. Considering that the Arctic amplification is a major threat to the Arctic region, in terms of permafrost degradation the soil will create more geotechnical problems, that require practical solutions and knowledge in a dynamic environment.

This study focuses on the extension of knowledge and interconnection between the local soil classification, thermal regime of the cast-in-place piles, and the adfreeeze shear strength at the concrete-soil interface. The current area of interest represents the Longyearbyen settlement, located in the Svalbard archipelago.

In order to determine the frozen soil characteristics, a series of laboratory tests are carried out at the University Center in Svalbard. By obtaining the soil classification as silty clay (SC) and silty sand (SM), including the stakeholders' analysis, the Sjoskrenten case study is presented as a discerning point for the objectives of the study.

The concrete behavior and soil-concrete bond is evaluated thoroughly for a further connection between the maturity and adfreeze bond variables. It has been observed that the lack of high maturity in the post-cast state of the concrete doesn't inevitably conclude to a relatively low adfreeze shear strength. Moreover, for the cast-in-place structures, the bonding response happens to have slightly better results than the compared specimens.

Furthermore, a recovery bond healing mechanism may be attributed to the roughness of the pile and water content between the soil-concrete interface.

The limitations of the laboratory analysis and lack of knowledge is assessed, consequently. Finally, data from the adfreeze design parameters and further recommendations can be used to improve the local design considerations.

Acknowledgement

The completion of this Master of Science thesis represents the ending point of the Cold Climate Engineering program. The current study was done under the Norwegian University of Science and Technology (NTNU) and University center in Svalbard (UNIS) umbrella, in collaboration with the Technical University of Denmark (DTU).

Initially, I would prefer to show my honest gratefulness for the thesis supervisors, respectively Associate Professor Aleksey Shestov (UNIS), Professor Gustav Grimstad (NTNU), and Associate Professor Thomas Ingeman-Nielsen (DTU). Their teaching approaches and supervision during the study and thesis period provided the cornerstone for the critical thinking and developing of a clear perspective on behalf of the Arctic relevant topics. The collaboration with the local stakeholders Hæhre Arctic and Multiconsult company gave fruitful results for the case study. Therefore, many thanks are given to Martin Nerhus Øen (Hæhre Arctic) and Lorenzo Cicchetti (Multiconsult).

As has been stated by many others before me, the sensitivity of the Arctic environment should become one of the priorities that are to govern our decision making, when we speak about the sustainable and infrastructure development. Therefore, many thanks to the Abbas Barabadi for the insights into the risk evaluation and the sustainable feature that the Arctic community is in need. Furthermore, I manifest my deepest gratitude to Gunvor Marie Kirkelund and Knut Vilhelm Høyland for the help, practical guidance, and believing into us.

Finally, many thanks and hugs for the dear persons that believed in me and my journey.

With genuine love,

Mihail Boescu 

Table of Contents

List of Figures

List of Tables

List of Abbreviations

ASTM-CS	American Society for Testing Materials Classification System
CIP	Cast-in-place
CL	Clay
DTU	Technical University of Denmark
FGE	Frozen Ground Engineering (book)
ISSCS	Indian Standard Soil Classification System
ISO	International Organization for Standardization
LL	Liquid Limit
LNSS	Leonhard Nilsen og Sønner Spitsbergen
MH	Inorganic silts, elastic silts
ML	Inorganic silts and very fine sand, silty of clayey fine sands or clayey silts with slight plasticity
NPRA	Norwegian Public Roads Administration
NTNU	The Norwegian University of Science and Technology
OL	Organic silts and organic silty clays of low plasticity
PI	Plasticity Index
PL	Plastic Limit
RCP	Representative Concentration Pathway
SC	Clayey sands, sand-clay mixtures
SM	Silty sands, sand-silt mixtures
SNSK	Store Norske Spitsbergen Kulkompani
UNIS	University center in Svalbard
USCS	Unified Soil Classification System
UWC	Unfrozen water content
W/C ratio	Water over Cement ratio
ZAA	Zero Annual Amplitude

Chapter 1: Introduction

Frozen ground is considered to be the soil or rock stratum with a temperature below 0 °C for a period of two years in a row. Frozen soil, however, represents the state in which the grains in combination with air, frozen and unfrozen water act as a bonded material, also referred as permafrost. The complexity of the four phased permafrost requires a thorough study of the rheological properties, that are governed and highly dependent on temperature, salinity, stress levels, grain size distribution, water content, and etc.

Frozen saline soils represent one of the challenges for the infrastructure design, in context of the dynamism of the Arctic. As they freeze at lower temperatures than the non-saline frozen soils, they are categorized between the frozen and unfrozen soils (Brouchkov, 2002). Moreover, a change in soil's strength and creep rate is strongly dependent on the salinity content, resulting in a reduction of its strength and increase in the creep rate for a higher presence of salt (Andersland et al., 2003). The long-term adfreezing strength for concrete and frozen saline soils also decreases linearly as the salinity content increases, leading to major continuous long-term deformations (Brouchkov, 2002).

For this study it is of a tremendous importance to mention the water-ice phase relationship in the context of a high salinity content that characterizes the area of interest. The strong dependency between the salinity and the Unfrozen Water Content (UWC) is deducted from the fact that an increase in the salinity is followed by an increase in the freezing point depression. The presence of salt in the soil pores is known to decrease the freezing point of the water located in the pores, that is causing a higher quantity of unfrozen water (MSc Morten Hovind, 2020). Therefore, the UWC varies in dependence to the quantity of solutes. On the other hand, the ice-water relationship also fluctuates in relation to the specific surface area of the grains, temperature, and mineral composition – resulting in different quantities of UWC for coarse- and fine-grained soils.

Considering the above, the thorough study of the local soils has a major contribution for the geotechnical engineering practices. Such companies as Multiconsult, and Hæhre Arctic manifest a need in knowledge in regard to the rheological properties of the soil, in terms of shear strength, interface adfreeze bond forces, temperature development, the method of pile foundation, and etc. Therefore, the construction practices, such as cast-in-place piles, have been deducted on the basis of the previous experiences and studies (e.g. Andersland et al., 2003), rather than on standards and procedures to which a contractor or stakeholder must stick in order to obtain a structural integrity and lower the environmental impact.

Moreover, the necessity of a temperature development assessment for the concrete plays an important role in the sustainable design of the geotechnical solutions. As the concrete slurry is affected by the temperature change and construction practices, the maturity of the foundation tends to vary actively. In terms of curing or freezing, the rate at which the maturity is obtained might be a major factor in the adfreeze strength bond. In order to have comprehensive conclusions about the curing of the slurry in a dynamic Arctic environment, one might analyze the outcome in respect to heat

propagation, the time required for a potential maturity, and the cement slurry composition.

Although a certain amount of information about the adfreeze bond strength is available in the specialized literature, few of the studies have been considering the local frozen saline soils. Therefore, dependency of the adfreeze strength to the ice saturation, creep rate, and temperature represents the aspect that must be considered in a precise analysis of the rheological properties, either in large scale observations or further studies, such as the current one.

1.1. Problem Statement

Svalbard is a Norwegian archipelago in the Arctic Ocean, that is located within a largely continuous permafrost zone (Olav, 1975). The five main settlements on Svalbard include Ny-Ålesund, Pyramiden, Longyearbyen, Barentsburg and Sveagruva. Developed as coal mining-related towns, today only Barentsburg and Longyearbyen are to a degree dependent on the mining activities. The main focus of the study will lay on the Longyearbyen town, with a population of 2368, that is the largest inhabited area in Svalbard.

During the historical development of the town, several foundation types were used, basically considering the conventional approach for stable soil and thermal conditions, as well as passive and active methods for thaw-unstable soil material (Humlum et al., 2003). For the structures built on the area of Svalbard, more emphasis was put on the passive approach (Humlum et al., 2003). One of the foundation types that has been used in the past included the wood piles, but due to the rotting process such type of application is rarely examined in the present, with exception of the impregnated timber piles (Sinitsyn et al., 2020).

Saline permafrost is dominant along the Arctic coastal regions, including Longyearbyen, that have been exposed to sea-level fall (Brouchkov, 2002). Located within a sedimented filled fjord area, the permafrost condition in Longyearbyen is characterized by ice poor to ice rich concentrations starting from the active layer (1m) up to five meters depth of the soil stratigraphy (Gilbert et al., 2019). Therefore, the soil freezing point differs widely from region to region, respectively between -0.1 $^{\circ}$C and -5.1 $^{\circ}$C (Gilbert et al., 2019). In addition, an engineering challenge will also come from the fact that “the pile load carrying capacities are reduced by at least 50 % at salinities as low as 5 ppt, by 60 % to 75 % at 10 ppt and by as much as 90 % at 15 ppt” (Biggar, 1991). The reduction of the load carrying capacity has been shown that is severe both in ice-rich and ice-poor saline frozen soil (Nixon and Neukirchner, 1984).

Considering the above-mentioned permafrost characteristics and the sensitivity of the local area, it is merely difficult to make a clear distinction between the effect of possible climate warming and other factors that could be affecting a structure on permafrost, such as wrong site and load assumptions, poorly made execution of the structure, and lack of proper maintenance (Humlum et al., 2003). Even though the predictions are showing that permafrost in Longyearbyen will be present after 2100, the temperature increase will cause poorer load-bearing capacity and increased settling rates (Istanes and L. Rongved, 2017). Current geotechnical issues are intensified by the arctic amplification as a climate change consequence (Schneider Von Deimling et al., 2021), therefore requiring a highly reliable and resilient infrastructure design, for example longer and larger in

diameter piles, an increased need in active type of foundation, and more incoming snowmelt and rainwater mitigation methods.

Under the pressure of necessity, the main goal of the study is to receive enough data in order to obtain a wide description of the local soils, and practices of foundation design. Moreover, it is important to observe the trends and parameters that could be investigated and used further on for the design or research processes.

1.2. Research Objectives

The current thesis considers bringing more knowledge and accuracy in terms of rheological properties for the saline frozen soil of the Longyearbyen area. Moreover, due to lack of extensive information in regard to the local construction practices (e.g. temperature development of cast-in-place piles) and adfreeze bond strength of the soil to pile interface, the main objectives of the study represent:

I. Proposing a basic classification and characteristics of the local soils with a focus on the stakeholder's interest.

II. Evaluation of the concrete piles' thermal regime in the post-cast state.

III. Studying of the rheological properties and behavior of frozen samples by means of shear and adfreeze bond on the local used piles in foundation design.

1.3. Research Methodology

Mechanical properties of the frozen soil samples are determined by means of cold laboratory and frozen state tests, that include shear measurements that could help at determining of the adfreeze strength of embedded piles, and uniaxial compression tests for the end-bearing strength of the soil. For the purposes and the outcome of this study the focus will lay on the adfreeze bond strength on marine saline permafrost with different ice and temperature conditions. The second part of the study represents an assessment of the temperature development of cast concrete in H-piles foundations, that are consistently used in Longyearbyen, specifically by Multiconsult company in the Folkeskollen project. Main interests of the stakeholders could be formulated as:

i. Hardening and curing of the cement slurry around the H steel pile.
ii. Heat of hydration and the maturity of the concrete.
iii. Quantifying the effect of heat transfer along the steel piles to the permafrost layer.

More conclusions could be drawn in regard to how the shear strength (adfreeze) is affected when adding the slurry, and if there is any point in adding the cement, instead of coarse-grained materials, or silty-clay fill. Also, problems could appear when the silty-clay fill thaws or hardens in case the ice content of the soil is considerably high. Furthermore, the perspective of sustainability and carbon emissions represents an important aspect of the second part of the study.

1.4. Thesis Structure

The outline of the current study is structured as follows:

- **Chapter 2: Theories and literature review**

Theoretical background on behalf of the frozen soil behavior considering the engineering design and influencing variables. The chapter presents the adfreeze bond strength mechanism and a thorough review of the concrete thermal development.

- **Chapter 3: Laboratory analysis**
  The chapter shows the characteristics and classification of the local soil, as well as the used methodology over the analysis. Results and classification of the AOI soil are evaluated.
- **Chapter 4: Case study – Sjoskrenten**
  In this chapter, the case study over the local stakeholders is presented and assessed. Soil classification, thermal behavior of concrete and adfreeze strength tests are investigated. Data implies the connection between all three aspects.
- **Chapter 5: Discussion**
  A critical discussion of the analysis and results of the previous sections is considered in this chapter. Mutual connection of the adfeeze bond and concrete cast-in-place behavior is evaluated.
- **Chapter 6: Conclusion**
  The ending chapter presents the main conclusions and recommendations in regard to the local soil behavior and construction practices.

Chapter 2: Theories and literature review

2.1. Frozen Soil state

Frozen soil (permafrost) is a four-phase material that consists of rock/soil matrix, ice, liquid unfrozen pore water, and air within the pore space. It represents the soil or rock with a temperature below 0°C for at least two consecutive years, that is distributed in the Arctic, sub-Arctic, and high-mountain regions (Andersland et al., 2003). Among the variety of the permafrost maps, the Circum-Arctic Map of Permafrost and Ground-Ice Conditions shows the permafrost extent, relative abundance and the location of subsea and relict permafrost in the Northern Hemisphere (20°N to 90°N) (Heginbottom et al., 2002). It is observed that for the Svalbard area, the dominant landforms are mountains, highlands, ridges, and plateaus characterized by thin overburden cover and exposed bedrock, as well as ice caps and glaciers. Generally, permafrost is divided between two specific zones, respectively continuous and discontinuous.

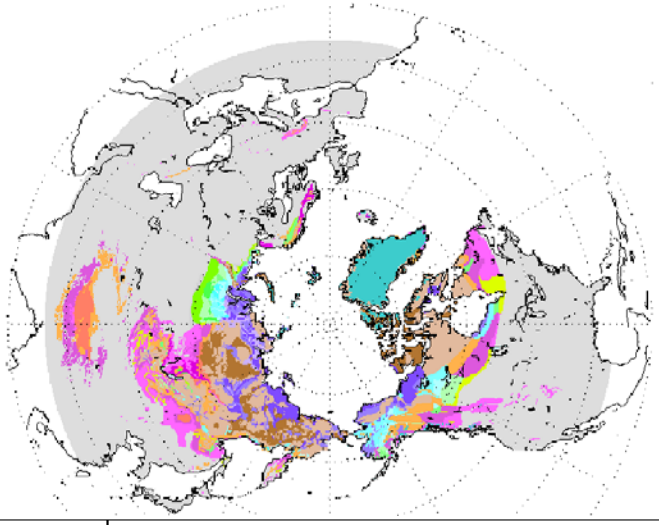

Permafrost Extent (percent of area)	Ground Ice Content (visible ice in the upper 10-20 m of the ground; percent by volume				
	Lowlands, highlands, and intra-and intermontane depressions characterized by thick overburden cover (>5-10m)			Mountains, highlands, ridges, and plateaus characterized by thin overburden cover (<5-10 m) and exposed bedrock)	
	High (> 20%)	Medium (10-20%)	Low (0-10%)	High to medium (>10%)	Low (0-10%)
Continuous (90-100%)	Ch	Cm	Cl	Ch	Cl
Discontinuous (50-90%)	Dh	Dm	Dl	Dh	Dl
Sporadic (10-50%)	Sh	Sm	Sl	Sh	Sl
Isolated Patches (0-10%)	Ih	Im	Il	Ih	Il

Variations in the extent of permafrost are shown by the different colors; variations in the amount of ground ice are shown by the different intensities of color. Letter codes assist in determining to which basic permafrost and ground ice class any particular unit belongs. Letter codes are defined in the documentation that accompanies the data files.

Ice caps and glaciers

Figure 2.1 Circum-Arctic Map of Permafrost and Ground-Ice Conditions (Heginbottom et al., 2002)

Another important surface to mention is the active layer, where the temperature is presenting positive and negative values during the year. The thickness of the active layer varies from place to place, depending on factors such as freezing index, material type, water content, vegetation, and slope characteristics (Andersland et al., 2003).

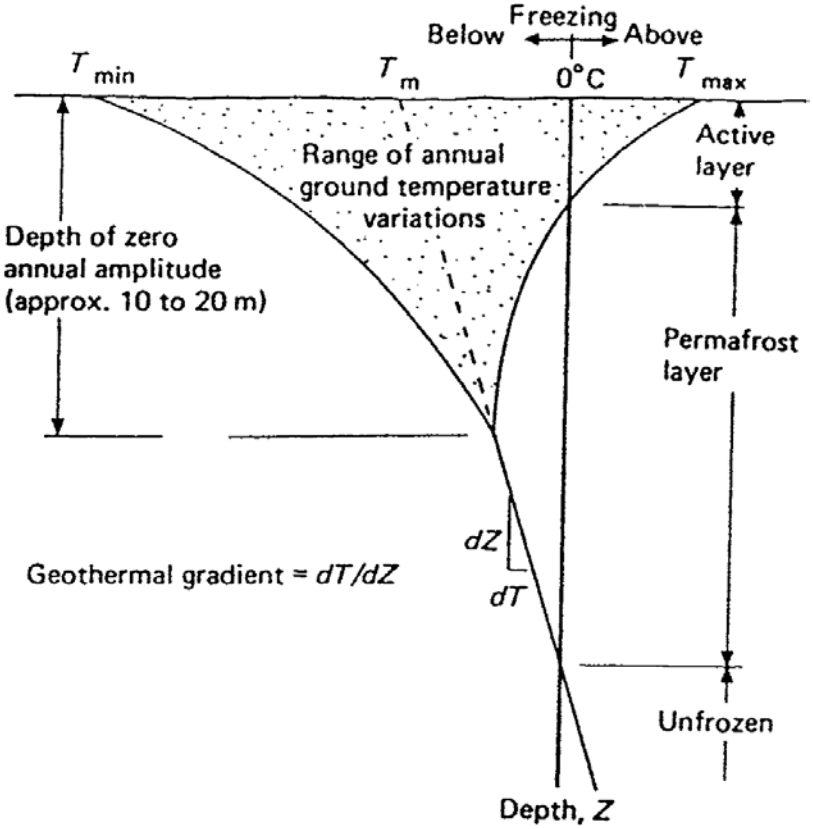

Figure 2.2 Temperature profile in perennially frozen soil (Andersland et al., 2003)

A more in-depth characterization of the frozen ground is presented by the trumpet curve in Figure 2.2, where the 0°C isotherm represents the distinction between the permafrost and the unfrozen layer. The mean annual temperature (T_m) is varying and dependent on the factors as described in the case of the active layer.

2.1.1.Permafrost engineering design

Foundation design in permafrost implies the optimization of the foundation type, regarding heat exchange and type of soil that is designed upon. For example, frost susceptible soils are prone to the expansion of the ice due to the high capillarity and permeability. Moreover, in the high permeability and low capillary rise soils, such as gravelly soils, ice segregation is merely a problem (Khalilzad and Sheshpari, 2016). On the other side, due to the low permeability and high capillary rise of the clayey soils, low amount of water and respectively ice lenses are stored. Geotechnically speaking, when the melting of the ice lenses happens, the settlement will occur, therefore causing little to severe damage to the structures embedded into permafrost (Khalilzad and Sheshpari, 2016).

From the construction engineering perspective, permafrost is having certain useful parameters, that are stability, high strength, and relatively good bearing capacity for the

structural loads (Andersland et al., 2003). But, when a structure is to be placed on/in the permafrost, the thermal regime is generally altered, therefore resulting in a heat exchange between the atmosphere and the soil. Knowing that the rheology of the permafrost is temperature dependent, by disturbing the temperature regime some of the above mentioned parameters will be deteriorating, including strength, foundation stability, deformation behavior, and potential settlement acceleration (Instanes, 2002). Moreover, according to the findings in the mechanicals response of the frozen soils, the interdependence between the ice matrix, strain rate, salinity and temperature controls the response of the stress-strain relationship and strength of the soil (Arenson et al., 2006). Ice, being a cohesive agent in the soil matrix, is causing an increase in the strength once the ice content decreases, due to the developed structural hindrance once the solid particles contact each other (Arenson et al., 2006). And due to the freezing point depression, that is causing an increase in UWC, the salinity has its own impact on decreasing the resistance of the soil. Respectively, for the design of the foundations it is of a tremendous importance to prioritize, first and foremost, the evaluation of the permafrost properties, rheology, and its behavior under specific thermal effects, UWC content and salinity. Considering that the design lifetime for structures in permafrost is between 30 and 50 years, the sensitivity of the soil with emphasis on the climate change scenarios is also a factor that must be subjected during the common engineering practices, e.g. annually updated design air thawing index and artificial cooling methods for the soil (Instanes, 2002).

In case of the foundation design, construction practices require either the pile type or slab foundation, in dependence to the frozen soil condition and requirements due to limitation of the heat loss. Furthermore, passive and active methods can be used for the mitigation of the last mentioned, heat loss. Some of the commonly used foundation types regarding the permafrost conditions can be observed in Figure 2.3.

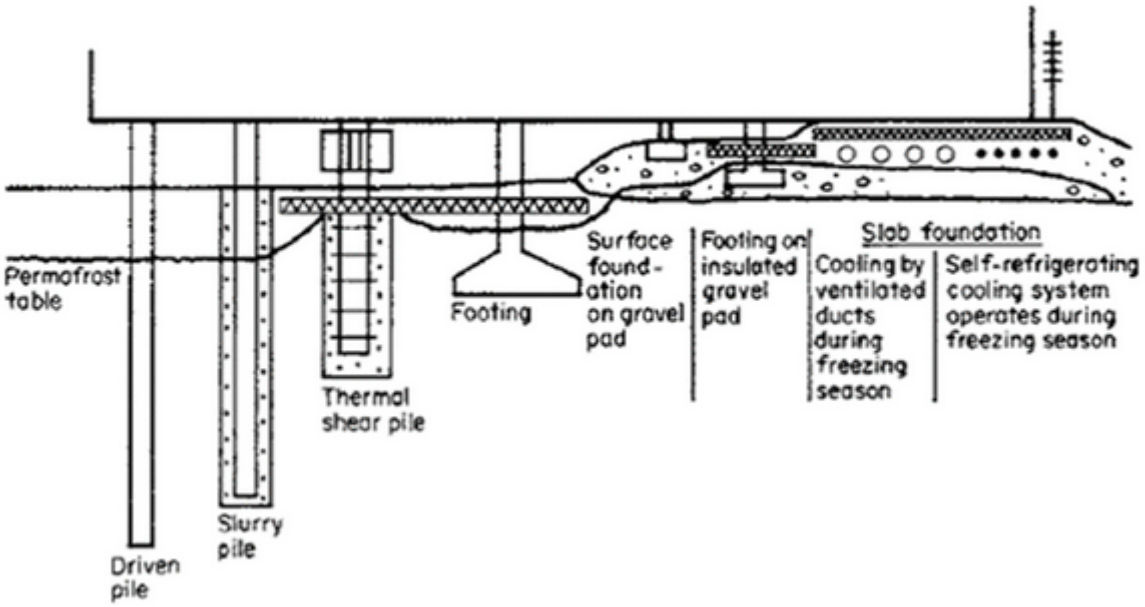

Figure 2.3 Permafrost type foundations (Eranti and Lee, 1983)

2.1.2.Permafrost Rheology

As mentioned in 2.1.1, the mechanical properties of the permafrost vary from case to case, depending on the temperature, unfrozen water content, salinity, and also the applied stress. Therefore, the strength of the soil will be relative during the year, in case of thaw-unstable soils especially, because it is losing strength as compared to the thawed values, plus it produces adverse and harmful settlements when it thaws (Barker and Thomas, 2013). Stress-strain behavior is considered to be similar to that of the ice (Arenson et al., 2006). Presented in an extensive study about the stress-strain behavior of the ice (Gold, 1970), the four possible response that are dependent on the applied strain rates are: A)ductile behavior with strain hardening, B)dilatant behavior with strain softening, C)brittle behavior with brittle failure just after yield point, D)brittle failure.

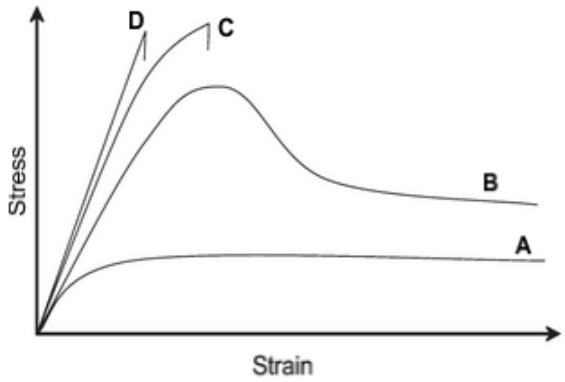

Figure 2.4 Stress-strain behavior for ice subject to a constant rate of strain. With increase in strain rate, behavior transforms from A) ductile behavior with strain hardening through to D)brittle failure (Gold, 1970)

Moreover, it is observed that the stress-strain behavior is a function of volumetric ice content, due to the solid soil grains that are influencing the stress-strain response (Arenson et al., 2006).

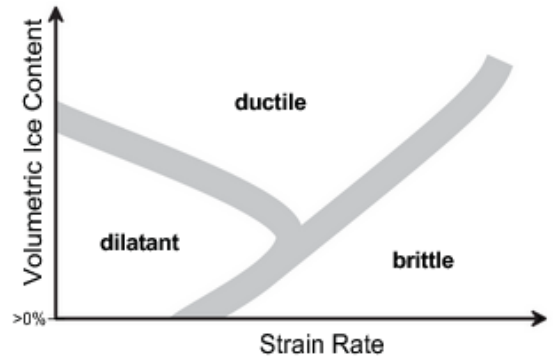

Figure 2.5 Stress response as a function of strain rate and volumetric ice content (Vyalov, 1963)

2.1.3.Unfrozen water

Water-ice frozen relationship holds a tremendous importance in the construction and engineering design in permafrost, due to the four-phase state of the frozen soil. Respectively, for a clear understanding of the soil properties, one step further is to study the unfrozen water content in the frozen soils. According to Andersland, the total water

content, w, in the soil is divided into two categories: unfrozen water, w_u, and ice, w_i (Andersland et al., 2003). Respectively:

$$\boldsymbol{w = w_u + w_i} \tag{1}$$

A power curve, as seen in Equation 2, is quantifying the unfrozen water content weight for specifically studied soils, by means of characteristic soil parameters α and β, and temperature θ.

$$\boldsymbol{w_u = \alpha \theta^{\beta}} \tag{2}$$

2.1.4.Salinity

The seashore processes and movement of the salt to the freezing front of clay soils have made the frozen saline deposits to become extensively distributed along the Arctic coasts (Brouchkov, 2002). One of the components that is having an impact over the freezing point depression is the salinity, and an increase in the salinity content will show an increase in the UWC. Moreover, the higher the presence of salt is, the less the soil is frost susceptible, resulting in a reduction of its strength and increase in creep rate at a specific temperature (Andersland et al., 2003). Many studies confirm that the compressive strength reduction and creep strains occurs often in the presence of solutes in the pore fluid, and only for an increase from 0 to 10 ppt in salinity the creep strain has the probability to raise dramatically (Brouchkov, 2002). Moreover, the cohesionless soil's compressive strength is related to the presence of UWC, that in many cases depends on the pore salinity of the soil, as mentioned in 2.1.1. Due to the sensitivity that the frozen soils possess in relation to the bearing capacity, the importance of the salinity in the design of the Arctic infrastructure embedded in permafrost becomes vital.

2.2. Adfreeze Bond Strength

The bearing capacity of a pile embedded into permafrost is totally dependent on the two mechanisms, respectively the end bearing and the adfreeze bond of the permafrost along the shaft or pile (Parameswaran, 1980). In some of the projects, the local private companies such as Multiconsult in Longyearbyen are having the designing practices based on the adfreeze bond strength, since the bedrock is at a high depth, and/or soil is not consolidated. Therefore, the adfreeze bond in the permafrost represents the major contributor to the local design practices.

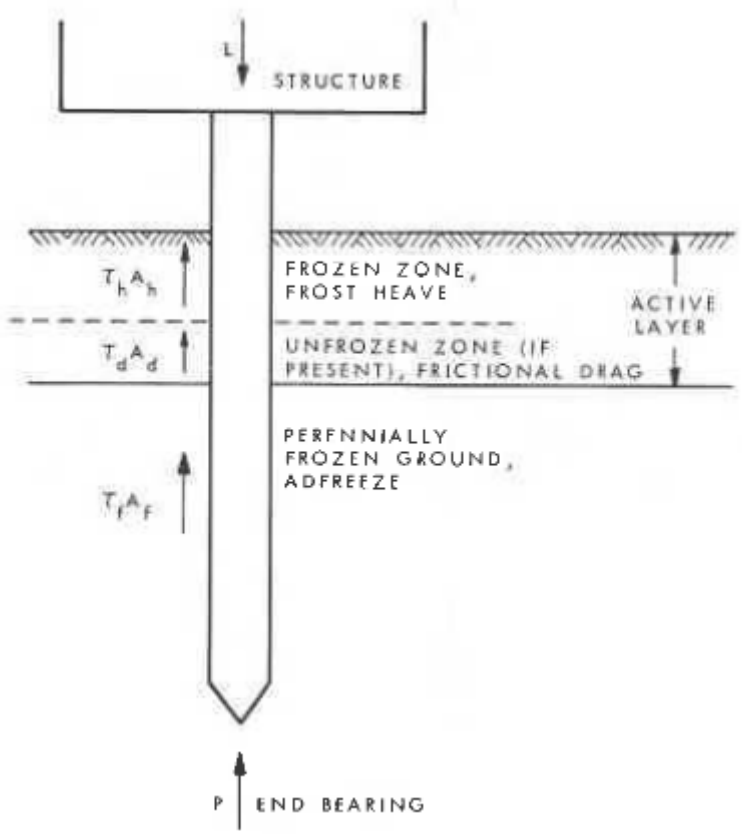

Figure 2.6 Schematic representation of forces acting on pile foundation in permafrost (Parameswaran, 1980)

It is considered that the following condition should be met, in order to obtain a stable and resistant pile-supported structure in permafrost (Parameswaran, 1980):

$$\boldsymbol{P + \tau_h A_h + \tau_d A_d + \tau_f A_f > L} \tag{3}$$

where *P* represents the end bearing capacity of the pile; τ_h - the frost heave stress in the frozen active layer; A_h - the pile-soil interfacial area in the frozen active layer; τ_d - the frictional drag stress (i.e., skin friction) between the pile and unfrozen soil (if present) in the active layer; A_d - the pile-soil interfacial area in this zone; τ_f - the adfreeze strength or shearing resistance at the pile-soil interface; A_f - the pile-soil interfacial area in the permafrost zone; and *L* - the structural load, and a combination of live loads: seismic, wind, construction loading, thermal expansion and contraction.

According to a research on the pile design in permafrost, the long-term adfreeze strength is mainly dependent on the soil temperature and type, and the roughness of the pile (J S Weaver and Morgenstern, 1981). Therefore, the adfreeze strength of a frozen soil, τ_a, is related to the long-term shear strength, τ_{lt}, respectively:

$$\tau_a = m\tau_{lt} \tag{4}$$

Where *m* represents parameter that characterizes the roughness and also takes into account the impurities of the pile. The long-term shear strength, τ_{lt}, consists of the frictional and cohesive components, according to the Mohr-Coulumb failure criterion:

$$\tau_{lt} = c_{lt} + \sigma \tan \phi_{lt} \tag{5}$$

Where c_{lt} is the cohesive component, ϕ_{lt} represents the frictional component, and σ is the normal stress on the shear plane (J S Weaver and Morgenstern, 1981). The authors are suggesting that the lateral stress is mainly small, less than 100kPa, and it should be neglected, therefore the Equation (4) should be noted as:

$$\tau_a = mc_{lt} \tag{6}$$

Moreover, according to an evaluation of the adfreeze bond of soil at -2˚C, it is being reported that the long-term shaft resistance depends also on residual angle of friction, ϕ_{lt}, and the normal lateral ground stress, $\sigma_{n,tot}$, (Ladanyi and Theriault, 1990), respectively:

$$\tau_{a,lt} = mc_{lt} + \sigma_{n,tot} tan\phi_{lt} \tag{7}$$

Which is implying that the long-term adfreeze strength is being influenced also by the frictional component, that may not have a relatively small value (Ladanyi and Theriault, 1990). In time of large pile settlements or pile driving in the frozen ground, the cohesive part is mainly reduced or destroyed, therefore the remaining residual strength comes from the residual friction (Andersland et al., 2003). The mentioned fact is that at a short period after the bond is being destroyed, the adhesive part of the adfreeze strength has a relatively low value, thus the frictional component represents the main pile capacity element (Andersland et al., 2003). The effect of the lateral stress may be considerable for the soils with large unfrozen water content, especially the saline soils in offshore permafrost areas (Ladanyi and Theriault, 1990). In some favorable conditions, as suggested, the portion of adfreeze against the pile surface could be recovered due to a bond-healing process as a result of water migration and refreezing in the pore space in contact with the pile, considering the presence of normal temperature, time and pressure (Ladanyi and Theriault, 1990).

2.3. Concrete thermal development in permafrost

Concrete, steel and wood pilling are usually one of the foundation methods used in the permafrost infrastructure engineering. Among the design approach, the type of designing method is chosen in dependence to the thawing regime of the frozen soil. Piling, in this case, can be used both for the passive and active method, respectively for permanent and temporary constructions (Andersland et al., 2003). In the specific situation of a concrete pilling method, they are used in the permafrost practice in pre-thawed and pre-drilled holes. Due to the development of high-alumina cement mix and high concentrations of calcium chloride mix (9-15%), the cast-in-place (CIP) pile method

started to become widely used in North American practices, as the grout will cure faster at low temperatures, such as -10˚C (Andersland et al., 2003).

The specific engineering issues for the practices that include the CIP method represent: (a) the slow rate of hydration of the concrete which will cause the freezing of the concrete, after which the refreezing of the ground will occur, and (b) the strength of the concrete will not be fully developed due to a low set rate of the concrete when frozen (Andersland et al., 2003).

2.3.1.Cement hydration

The concrete hydration has a considerable effect on the temperature development of the concrete, as well as on the permafrost-concrete interface bond. The thermal development of concrete can be constituted by having certain values about concrete and air temperature, type of cement, and content of the cement in the mixture.

The hydration process represents a concomitant exothermic reaction of the several compounds of cement with water. However, the clinker elements are having a different hydration speed, therefore at the end of hydration the following characteristics can be observed:

Clinker mineral	C_3S	C_2S	C_3A	C_4AF
Heat of hydration Btu/lb	215	110	310	130

Figure 2.7 Heat of hydration for the four clinker minerals (Rasmussen et al., 1989)

The reference temperature is 23˚C for a W/C ratio of 0.45 and a Blaine fineness of 3100 cm^2/g.

Knowledge in regard to heat release, and reaction speed is valuable because it tells about the setting time, hardening of the cement, and action on the hydration (heat progresses or slows down) (Mehta and Monteiro, 2014). Figure 2.8 shows the five stages of the heat evolution of hydration of cement under controlled conditions.

In the Stage 1 (Initial, or the dissolution stage) a rapid heat evolution that stays for several minutes is happening due to the hydration of alite, and heat of aluminates and sulfates (C_3S and C_3A) (Mehta and Monteiro, 2014). Decrease in heat happens because of the solubility of aluminates that is lowered due to the presence of the sulfates.

In the second Stage (Induction) the rapid concentration of ions are built on the alite solution, by limiting access to water, and therefore is also called dormant stage (Sedaghat, 2016).

Stage 3 represents the heat of formation of ettringite. Acceleration Stage takes place with a greater amount of time than the previous stages, as it depends on the presence of growing regions of C-S-H to give high hydration rate (Sedaghat, 2016), and includes some heat of solution due to also C_3S (Mehta and Monteiro, 2014). Initial set will show up in and the beginning of solidification of the paste will take place before the peak.

In the Stage 4 (Deceleration), by reaching the top of the curve (after 6-8 hours) the final set will happen and the hardening process will start (Mehta and Monteiro, 2014). The thickening of the paste reduces the heat flow, and the amount of ions passing are therefore reduced with time (Sedaghat, 2016).

Stage 5 denominates the end of the hydration process, with the concrete reaching the steady behavior. The released heat is the same as for the induction stage, and the space that water occupied is now covered with the hydrated cement, therefore the hydration process is lowering the heat evolution drastically.

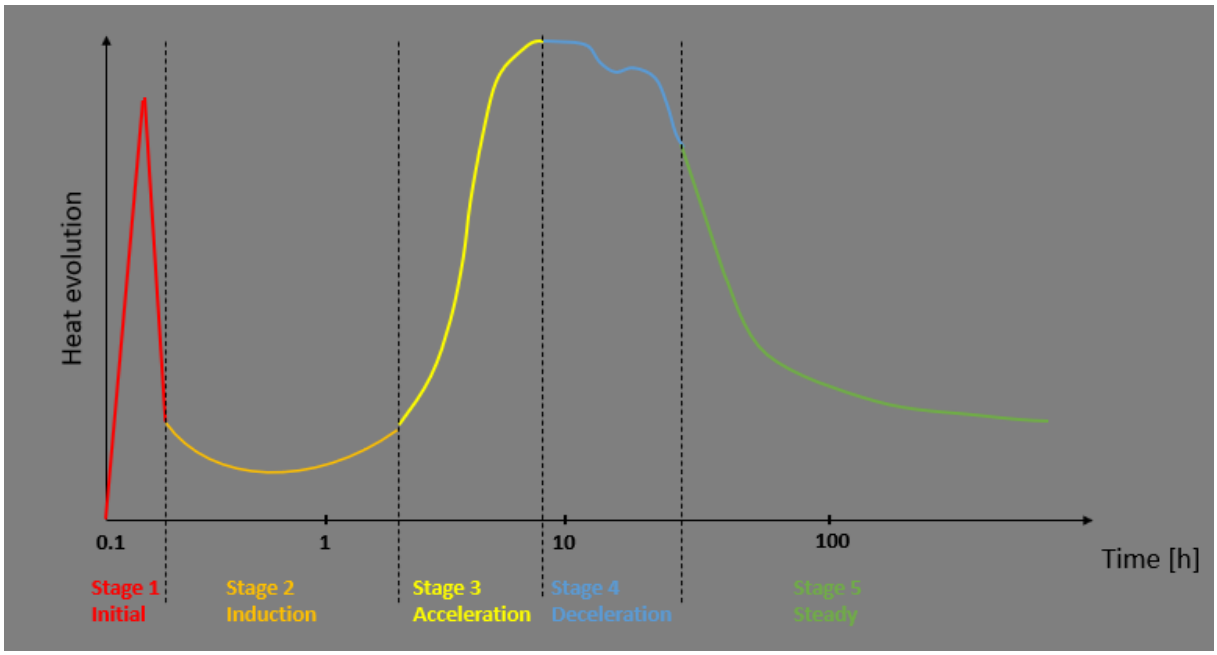

Figure 2.8 Schematic illustration of the Mechanism of heat of hydration of Portland cement. Reproduced on the basis of (Sedaghat, 2016)

For the ongoing practices in the frozen soils, and especially for marginal or concrete sections thinner than 250mm where the heat of hydration is dissipated more rapidly, the heat of hydration and/or the curing rate can be increased by using one of the following components: lower water-cement ratio (it lowers the degree of large pores in the hydrated cement paste, and also there will be less internal pressure due to supercooled water in the gel pores that is not flowing toward the ice in the capillaries (Mehta and Monteiro, 2014)), richer mix design, high early or regulated-set cement, accelerating additives, or the mentioned high-alumina, and high calcium chloride concentrated mixes (Andersland et al., 2003).

2.3.2.Flow of heat

Hydration of cement has a high degree of complexity, and therefore to cover all of the elements that participate at the reaction, such as fineness, clinkers distribution, temperature rise, parameter expressing the water availability, and mutual interaction, several models are considered to be available, such as Kishi and Maekawa model, Byfors model, De Schutter and Taerwe model, Freiesleben Hansen and Pedersen, and Pane models (Wang et al., 2006). Generally, the flow of heat in concrete is determined by the

Fourier equation, which has the following two-dimensional form (Ballim and Graham, 2004):

$$\boldsymbol{\rho \cdot C_p \cdot \frac{\partial T}{\partial t} = k \cdot \left(\frac{\partial^2 T}{\partial x^2} + \frac{\partial^2 T}{\partial y^2}\right) + \left|\frac{\partial q}{\partial t}\right|}$$

(8)

Where:

ρ : concrete density, (Kg/m^3)

C_p : specific heat capacity of concrete, (Kcal/Kg · °C)

T : temperature, (°C)

t : time, (hours)

k : thermal conductivity of the concrete, (Kcal/m ·hr · °C)

x, y: the coordinates at a particular point in a structure, (m)

q : internal heat evolved per unit volume, (Kcal/m^3·h)

$\left|\frac{\partial q}{\partial t}\right|$: time rate of heat evolution at point (x,y) in the structure.

As solution for the Equation(8), total heat per unit mas of binder, q , is considered as an input, which is a time dependent component, respectively:

$$q = C_p \cdot (T_t - T_0)\frac{m_s}{m_c}$$

(9)

Where:

C_p : specific heat capacity of the concrete, (Kcal/Kg · °C)

T_t : temperature of the concrete sample at time t, (°C)

T_0 : temperature at the beginning of the measurement/test, (°C)

m_s : mass of the concrete sample, (Kg)

m_s : mass of the cementitious material in the concrete sample, (Kg)

The rate of evolution of heat is determined by considering the numerical differentiation of time:

$$\frac{\partial q}{\partial t} = \frac{\delta q}{\delta t}$$

(10)

2.3.3.Maturity age of concrete

The rate of hydration is increasing with the temperature, therefore the development of the concrete properties cannot be described generally as a function of time. The rate of evolution of heat will vary at different sections in the structure, since not all the points in the concrete element are having the same behavior, in respect to time-temperature evolution (Ballim and Graham, 2004).

The concept of maturity age is introduced as the equivalent age (or time of hydration) at a reference temperature (Just Andersen et al., 1992). Therefore, the heat evolution is expressed in the maturity form, according to an approach of (Ballim and Graham, 2003):

$$M = \sum_{i=1}^{i=n} exp\left[\left(\frac{E}{R}\right)\left(\frac{1}{293} - \frac{1}{273 + 0.5 \cdot (T_i - T_{i-1})}\right)\right] \cdot (t_i - t_{i-1}) \tag{11}$$

Where:

M : equivalent maturity age for the reference concrete cured at 20°C, expressed as t_{20} hours (Ballim and Graham, 2004)

E : the activation energy parameter, (33.5KJ/mole)

R : the universal gas constant, (8.314J/mole)

T_i : the temperature at the end of the i-th interval, (°C)

t_i : clock time at the end of the i-th interval, (h)

According to the literature, the heat evolution rate can be normalized by expressing it as a maturity rate of heat evolution (Ballim and Graham, 2004). The form of the equation can then be used as an input solution for Equation (8):

$$\frac{\partial q}{\partial M} \tag{12}$$

Considering the time and each point in the concrete structure, the heat evolution rate can be determined:

$$\frac{\partial q}{\partial t} = \frac{\partial q}{\partial M} \cdot \frac{dM}{dt} \tag{13}$$

As an example of relationship between the heat evolution rate and maturity of concrete, a study suggests the following equations (Wang and Dilger, 1994):

$$\dot{q}_t = 0.5 + 0.54M^{0.5}, for\ M \leq 10hours$$

$$\dot{q}_t = 2.2exp[-0.0286(M-10)], for\ M \geq 10hours \quad (14)$$

Where *M* represents the maturity of the concrete relative to the concrete that is cured at 20 ˚C and heat evolution is expressed in W/kg of cement.

2.4. Summary

As mentioned by the studies, the examination of the possibility of mixing of the fresh concrete with the soil should be an important aspect, as it may cause lower strength concrete and weaker adfreeze strength at the soil-pile interface (Weaver, 1979). Due to a slow curing of the concrete, the hydration could interfere with the mixing of concrete and frozen soil, that has been observed at permafrost temperatures of -3˚C and concrete cast temperatures of +5˚C, that is also a case study of the current thesis. Nonetheless, the thawed zone of saline soil, that may be created around the casted concrete, could sufficiently increase the roughness of the pile (Weaver, 1979).

Moreover, due to the changes in temperature of the permafrost, the strength of the adfreeze bond will have considerable changes, being one of the main concerns that engineers are facing with (Istanes et al., 2005). Considering the saline or sensitive permafrost areas with temperatures that are close to the melting point, the heat generated by the CIP pile foundations will affect the load capacity of the infrastructure (Hou et al., 2022). Therefore, it is of a tremendous importance to consider the thermal behavior of concrete in the adfreeze strength and stability of a structure.

Chapter 3: Laboratory analysis

3.1. General background

Figure 3.1 General map of Svalbard (Norwegian Polar Insitute, n.d.)

Longyearbyen town is positioned in the Svalbard's archipelago, Spitzbergen Island, that is shown in Figure 3.1. The settlement is located within the Longyeardalen valley, that is predominantly characterized by marine, glaciofluvial and morainic deposits (see Figure A.1 and Figure A.2 for the geological aspect).

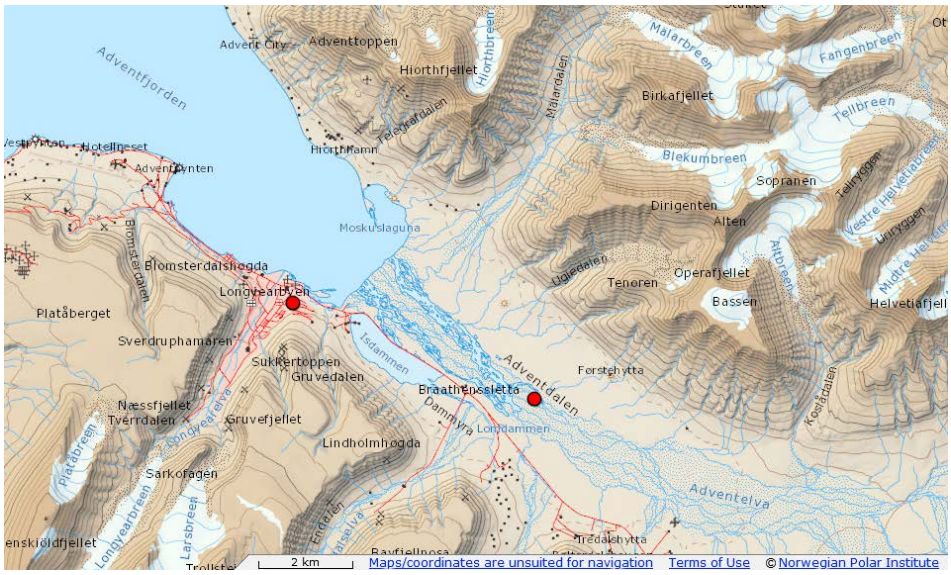

Figure 3.2 Previous sample site locations (Norwegian Polar Insitute, n.d.)

UNIS East and Adventdalen field sites (see Figure 3.2) represent among others the area of interest for the past studies on the local soil characterization. A variety of local areas are also considered for private ground investigations in the initial phase planning of different infrastructure projects in Longyearbyen (e.g. Gilbert et al., 2019, Pedersen, 2017, and Domaas et al., 2017).

3.1.1.Climate Data

Longyearbyen town is located in a so called polar tundra desert, with long, cold winters and short, cool summers (Gilbert et al., 2018). Due to the Arctic amplification and local anomalies, it is observed in Figure 3.3 that the mean annual temperature in Svalbard has been increasing from −6.8 °C in 1989 to −3.9 °C in 2018 (Gilbert et al., 2019). Moreover, it was observed an increase in the thawing index from approximately 400 °C·days to 575 °C·days, as well as a decrease in the air freezing index from approximately 2850 °C·days in 1989 to 2000 °C·days in 2018 (Gilbert et al., 2019).

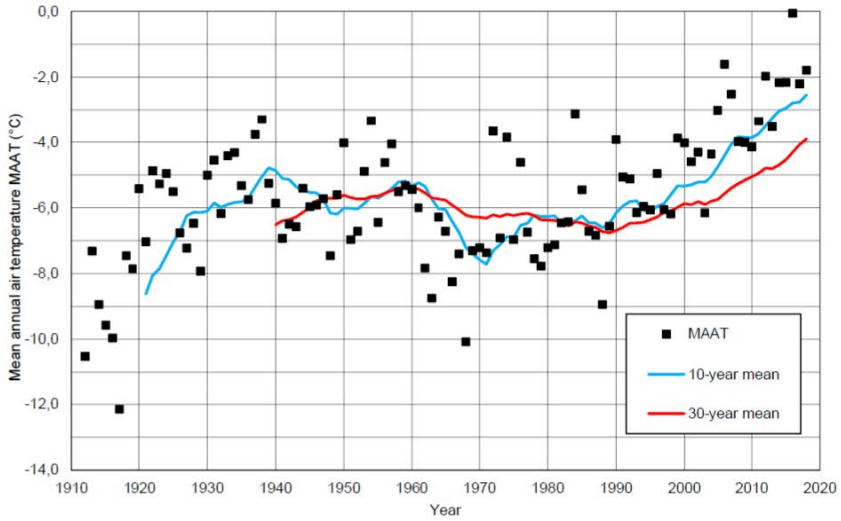

Figure 3.3 Mean annual air temperature Longyearbyen, Svalbard (Gilbert et al., 2019)

According to the predictions made by the modelling of the climate data for RCP 4.5, five data series are being received in a recent study (Istanes and L. Rongved, 2017), which is further compared to the historical data that is available. The mean annual temperature is seen to correspond with a moderate increase, respectively with 4°C to 9°C increase in 2100, as compared to present.

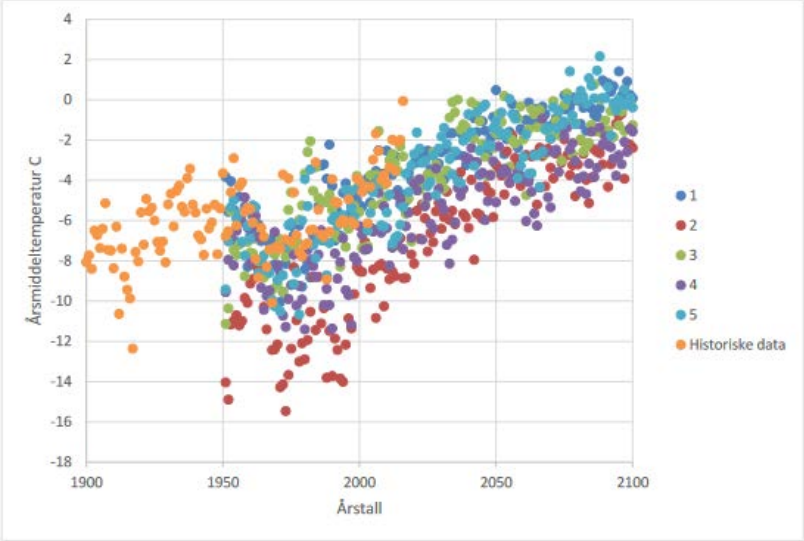

Figure 3.4 Modeled Annual Temperature based on RCP 4.5 for 5 data series (Istanes and L. Rongved, 2017)

Figure 3.5 and Figure 3.6 show the Air freeze and Air thawing indices modelling, based on seasonal mean temperatures for the RCP 8.5 (Bekele and Sinitsyn, 2020). It is observed that after the year of 2080, seasonal mean temperature presents positive values.

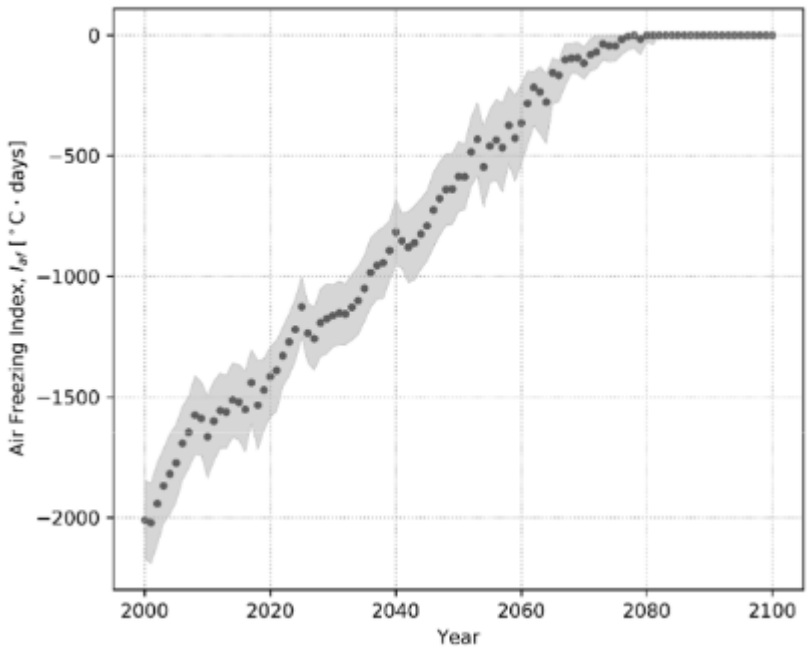

Figure 3.5 Air freezing indices based on seasonal mean temperatures (Bekele and Sinitsyn, 2020)

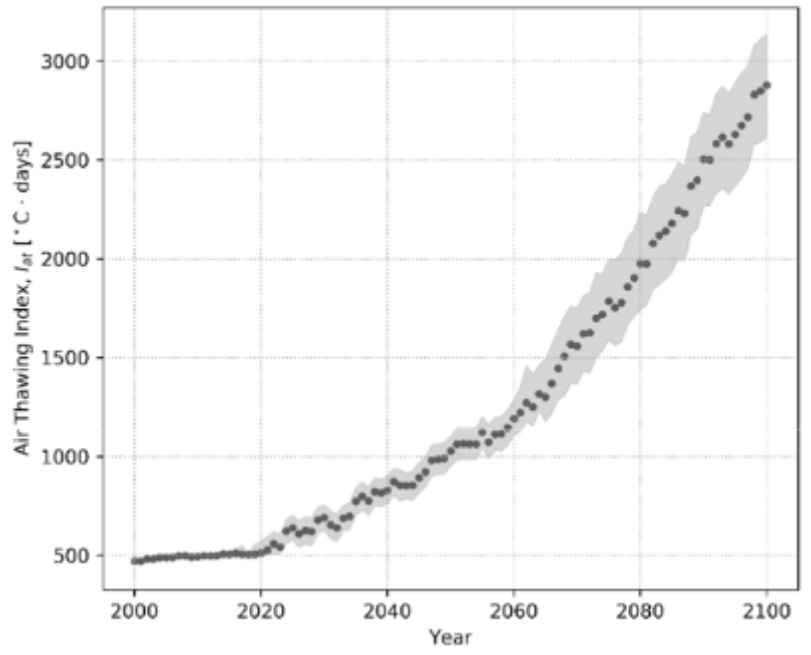

Figure 3.6 Air thawing indices based on seasonal mean temperatures (Bekele and Sinitsyn, 2020)

Considering the above-mentioned climate observations and models for the climate change, the local geotechnical problems and natural hazards will increasingly be predominant. A range of positive feedback loops related to the climate change will cause damage to the infrastructure and cultural protected heritage. Respectively, concerns for the stability in time of the infrastructure in Longyearbyen are becoming a reference for the on-going studies and analysis (Istanes and Rongved, 2019).

3.1.2.Stratigraphy aspects

The settlement is located along the bank of Longyeardalen on the shore of Adventfjorden, and mouth of Adventdalen. At the end of the Longyeardalen, glaciers Longyearbreen and Larsbreen are located. As it was mentioned, the town area is situated within a sedimented filled fjord area. Particular trends for the stratigraphy indicate silt or silty clay of low plasticity (OL) with water content of more than 50% and low salinity concentrations (0.08%) for the first 1.5m, inorganic silt or clay (ML-CL) with water content of 20 to 25% and salinity of 0.6 % for the 1.5 to 3.0m depth, and sand with fines (SM or SC) with relatively 15 to 25% water content and salinity of 0.3% for the further depths of 3.0 to 4.0m. The description is referred to a recent study done at Lea, close to the Building 33 on veg 236 (Bekele and Sinitsyn, 2020). Moreover, another investigation carried out at the Svalbard Research Park (in the alluvial sediments area) indicates that for a profile of 15m of borehole, the first 2-2.5m are characterized by gravelly, sandy, silty soil material with low water content (10%) and salt content of 2- 4 g/l (NGI, 2002). The water content was found to be 20-30% and the salinity of up to 35g/l at depth -2m. The ice was present at depths of up to 10m in several regions.

The permafrost in Longyearbyen is continuous, with unfrozen layer of 0.5 to 3.0m in thickness. It is considered that the active layer is thin in unconsolidated sediments, and thick in solid rock (Winfried, 2015). A Multiconsult's surveys also validates the thickness of the active layer of up to 3.0 m (Hannus, 2016). The depth to bedrock in the case of the UNIS East ranges from 21m to 30m (Gilbert et al., 2019).

Modelling-based predictions show that by 2050 the active layer may increase by 10-20 cm (Etzelmüller et al., 2011) Another estimations of the active layer thickness for 2100 show that it will increase from values of 1.5m to 2.5m, respectively by an approximation of 60% in size (Istanes and L. Rongved, 2017). Both the studies indicate that major degradation for the permafrost is not expected for the areas with no ground disturbance by human activities. Even though the surface temperature is increasing by year 2100, predictions conclude that at depths of 10-20m temperature will have values of -2°C to -3°C (Istanes and L. Rongved, 2017).

Considering the above-described stratigraphy and predictions for the active layer increase within a climate warming scenario, the impact will be distributed generally onto two specific areas: ice dominant layer and high saline layer that is situated within the top few meters of the permafrost. It is important to mention here that the high saline content of the pore water decreases its freezing point, and therefore the increase in unfrozen water content is expected (Instanes & Instanes 1999). From a geotechnical design perspective, the saline pore water is responsible for several consequences: it is influencing the bearing capacity of the foundations; it is increasing the deformation susceptibility of both the permafrost and foundation; and due to the positive feedback loop of high salinity and permafrost melting mentioned above, it causes an increase in creep rates of existing foundations such as piles and footings, as well as increased creep of embankment foundations (Humlum et al., 2003 and Gilbert et al., 2019). Specifically for piles embeded in permafrost, the adfreeze bond between the pile and frozen soil is significantly reduced due to the saline pore water content (Humlum et al., 2003). Respectively, any future warming of the permafrost in highly sensitive areas such as Longyearbyen will cause substantial issues for the local infrastructure.

3.2. Soil classification

The laboratory investigation was done in parallel with the UNIS course AT-205 class - Frozen Ground Engineering for Arctic Infrastructures. The drilling operation has been executed at the UNIS East site with assistance of Multiconsult company (see Figure 3.2 for the general location and Figure A.3 for a field photo). Different core segments were used for the following laboratory work: uniaxial compression and creep tests, measurements of salinity, grain size distribution and water content, and Atterberg limits (plastic and liquid).

3.2.1.Water content

Water content (or gravimetric water content) represents the ratio between the weight of water and the weight of solids in a soil specimen. After drying at 110°C for 24 hours, samples are cooled down and weighted. Respectively:

$$w\,[\%] = \frac{W_w}{W_s} \cdot 100\% \tag{15}$$

3.2.2.Salinity

Salinity was measured directly from the water that the soil sample was presenting, therefore a higher water content sample was used. With a salinity refractometer, the saline percentage is shown [%]

3.2.3.Atterberg limits

The liquid and plastic limits represent the Atterberg limits. As the soil dries uniformly after a fully saturated state, the water and volume of the soil is reducing. Therefore, we can deduce the boundaries of the soil as it transits the liquid, plastic, semisolid, and solid states that are related to the physical and mechanical behavior of fine-grained soils, as seen in the following figure:

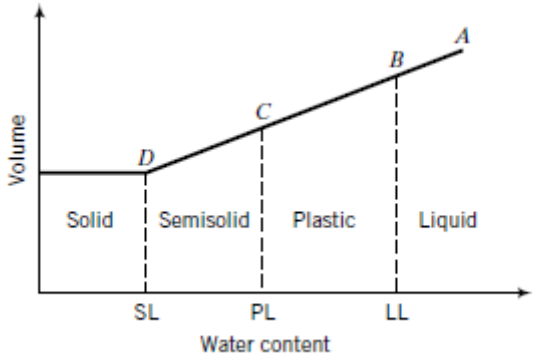

Figure 3.7 Changes in soil states as a function of soil volume and water content (Budhu, 2010)

Liquid limit

Liquid limit is considered as the limit where the soil is behaving fully liquid. For the purposes of our analysis, liquid limit was determined by Casagrande method, following the ISO 17892-12 (ISO, 2018). Liquid limit is determined on the fine-grained soil that is achieved after sieving through 0.425 mm mesh. A portion of the dry soil is mixed with distilled water and placed in a special cup where it has to reach a thickness of 12.5 mm approximatively. After smoothing of the surface, a groove is cut into soil with a standard grooving tool (see Figure 3.8). The speed of the rotation has to be done for 2 revolution per second until the groove will close over a length of 12.5 mm. The numbers of blows are counted, and the water content is determined further on.

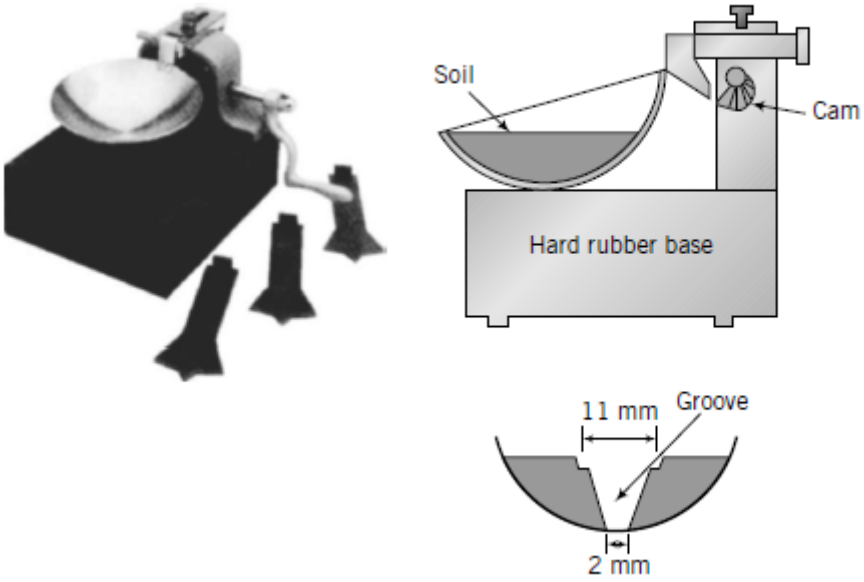

Figure 3.8 Cup apparatus for the determination of liquid limit (Budhu, 2010)

Liquid limit is defined as the water content of the soil at which the groove closes over a length of 12.5 mm and reaches 25 blows of the Casagrande apparatus (Budhu, 2010). After obtaining a series of results for the number of blows and water content of the specimen, the results are presented in a plot of water content (arithmetic scale) versus terminal bowls (logarithmic scale), from which the liquid limit is read:

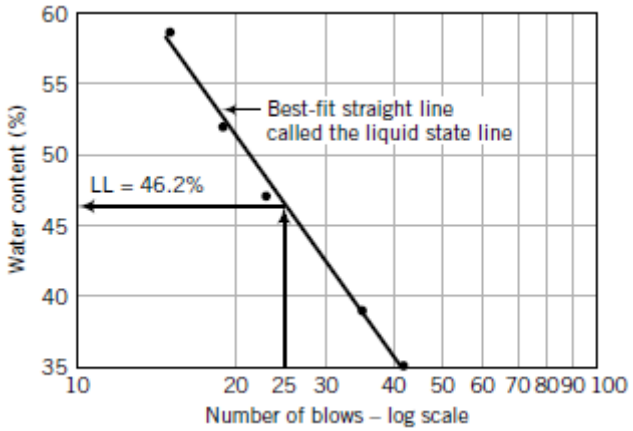

Figure 3.9 Typical liquid limit results from the Casagrande cup method (Budhu, 2010)

Plastic limit

Investigation of the plastic limit will be performed according to the approved standards, e.g. ISO 17892-12 (ISO, 2018) - the disk rolling method in which a soil specimen is rolled on a preferably porous plate, until it reaches a diameter size of 3 mm and starts to crumble into pieces. The plastic limit is found to be the water content of the sample, which can be measured as for the previous samples. Considering the plastic and liquid limit, multiple factors can be calculated, from which are the Plastic index (I_P), Liquid index (I_L), and Consistency index (I_C).

$$I_P\,[\%] = w_L - w_P \tag{16}$$

$$I_L\,[-] = \frac{w - w_p}{w_L - w_P} \tag{17}$$

$$I_C\,[-] = \frac{w_L - w}{w_L - w_P} \tag{18}$$

3.2.4.Fall cone test - shear strength of soil

The standard ISO 17892–6 refers to the estimation of the shear strength values by the fall cone test, as well as using other methods (ISO, 2017). Developed by Mr. Sven Hansbo, the method is used for estimating the undrained shear strength of the soil, τ_f :

$$\tau_f = KQ/h^2 \tag{19}$$

Where K depends mainly on the cone angle but is also influenced by the rate of shear and sensitivity, h represents the depth of penetration, and Q is the weight of the cone (Hansbo, 1958). The laboratory tests were done on both undisturbed and remodeled soil samples. Undisturbed samples were considered too frozen and hard in order to reach a considerable penetration, therefore the test is reliable with the unfrozen samples.

Sensitivity of the soil can be determined with the Fall Cone apparatus, that gives us a quick and reliable empirical value:

$$S_t = \frac{c_u}{c_r} \tag{20}$$

Where c_u represents the undisturbed shear stress, and c_r is the remodeled shear stress For the values of the sensitivity, clay is qualified as slightly sensitive [0;8], averagely sensitive [8;30], and very sensitive [30; ∞].

3.2.5.Grain size distribution

For the dimensions of higher than 0.075 mm grain size distribution is done by means of mechanical sieving. For the grain size less than 0.075 mm the distribution was done by using the sedimentation analysis. Sedimentation method follows the standard for sedimentation test ISO 17892-4 (ISO, 2016), however for the test method we used a hydrometer sensor and a distribution model by Stokes' law regarding the sedimentation of spheres. As the time passes and the settlement of the particles takes place, the density of the water changes that can be measured at established points in time. Results of the sedimentation test consists in determining of the fine-grained soil smaller than 0.075mm and classifying it as clay or silt.

3.2.6.Results and discussion

Results will be reproduced from the group's results that have been obtained along the investigation of the specimens:

Water content

Group 1 Sample 7 (2.1m)	Group 2 Sample 3 (2.55m)	Group 2 Sample 7 (2.85m)	Group 2 Sample 10 (3.05m)
24.90 %	15.20 %	4.20 %	12.90 %

Table 3-1 Water content of the tested soil

Water content for the examined samples shows different values for an interval of approximatively 1m of permafrost, respectively from 4.2% to 24,9%.

Salinity

Group 1 Sample 5 (1.95m)	Group 2 Sample 2 (2.50m)	Group 2 Sample 9 (3.00m)	Group 2 Sample 11 (3.10m)
1.00 %	2.00 %	2.10 %	0.80 %

Table 3-2 Measured salinity values

The salinity measurements have 2 distinct values, for the samples with visible ice lenses (approx. 1%) and for the samples with a higher portion of soil (approx. 2%). It could be assumed that the layer between 2.05m and 3.10m has a higher concentration of salts due to less water content represented as ice and due to more UWC in the pores of the soil. Otherwise, a higher degree of precision over the measurements had to be considered, with a considerable number of values.

Bulk density

	Sample #	Depth range [m]	Bulk density average [g/cm³]
Gr1	4,9,10	1.90-2.02; 2.15-2.39;	1.89
Gr2	5,6	2.65-2.85	1.91

Table 3-3 Calculated bulk density

Bulk density for different depth ranges was calculated and an average of it is concluded, with a slightly larger bulk density for the lower layers.

Liquid limit

Sample	Blows[-]	Bowl mass[g]	Bowl and soil mass wet[g]	Bowl and soil mass dry[g]	Water content[%]
1 – 2	24	25.00	45.60	42.40	**18.39**
1 – 1	15	24.00	49.00	44.30	23.15
2 – 1	32	23.00	54.00	50.00	14.81
3 – 1	42	24.00	43.00	39.82	20.10

Table 3-4 Liquid limit results

Water content values do not represent the liquid limit of the soil, except for the sample 1-2 that has a value of 18.39% for 24 blows. The accuracy of the tests is not highly reliable as Casagrande Cup method has a difficulty in order to achieve a L.L. for a low number of tests and not properly sieved soils, and it has many drawbacks including: the tendency of low plasticity soils to slide and to liquefy as long as there is the shock, rather than flowing plastically; and the high sensitivity of the test due to the operator technique, speed of blow (2 revolutions/second), and apparatus differences (Hansbo, 1958).

Plastic limit

Sample	Bowl mass[g]	Bowl and soil mass wet [g]	Bowl and soil mass dry[g]	Water content[%]
1	21.02	22.18 w lid	22.02	16.00
2	14.40	16.39	16.13	15.03
3	12.97	15.64	15.27	16.09
Average plastic limit				**15.70**

Table 3-5 Plastic limit

For the plastic limit of the specimen an average value was subtracted out of the executed tests, respectively 15.70 %.

Sensitivity and Undrained shear strength

Group 1: 2,4m depth				Group 2: 3,2m depth			
	Depression [mm]	Mean Depression [mm]	Shear Strength [kPa]		Depression [mm]	Mean Depression [mm]	Shear Strength [kPa]
Undisturbed (100g/30°)	7.00 6.00 7.00	6.66	c_u = 26 .00 τ_f = 22.11	Undisturbed (400g/30°)	3.50 3.00 2.50	3.00	c_u = 275.00 τ_f = 435.85
Remodeled (100g/30°)	10.50 11.00 9.00	10.16	c_s = 11.30 τ_f = 9.50	Remodeled (100g/30°)	4.25 3.50 1.50	3.10	c_s = 71.60 τ_f = 102.05
Sensitivity	2.30 = Slightly sensitive			Sensitivity	3.80 = Slightly sensitive		

Table 3-6 Shear strength and Sensitivity results

Shear strength of undisturbed and remodeled clay are being reported according to the values that are peculiar to the angle of the cone and depression made by it. Soil samples are classified as slightly sensitive. Besides taking the values from the supporting material, undrained shear strength, τ_f, was calculated manually. The K factor that depends on the angle of the cone, was selected as 1.00 for 30˚ cone for both undisturbed and remodeled soil. Therefore, we observe relatively big differences for the undisturbed sample (400g/30°). The difference could come from the fact that the soil was frozen in its undisturbed state, therefore stiff enough in order to not to be penetrated, even though the cone was of a higher weight as compared to the other tested samples. The investigations and literature, however, do not take into account or consider the frozen state of the soil, but rather apply the tests on the unfrozen clay (Hansbo, 1958). For our purposes, the remodeled soil was in the unfrozen state.

Grain size distribution

Sieve no. material in sieve	Sieve grid size[mm]	Tin mass[g]	Tin + soil mass[g]	Mass of solids [g]
4	4.750			0.14
8	2.360	5.92	6.14	0.20
16	1.180	5.90	6.59	0.70
30	0.600	13.80	17.05	3.30
50	0.300	14.00	98.41	84.40
100	0.150	13.60	88.39	74.80
200	0.075	13.50	137.82	124.30
Bowl(tail)	<0.075	480.00	735.25	255.25

Table 3-7 Grain size distribution

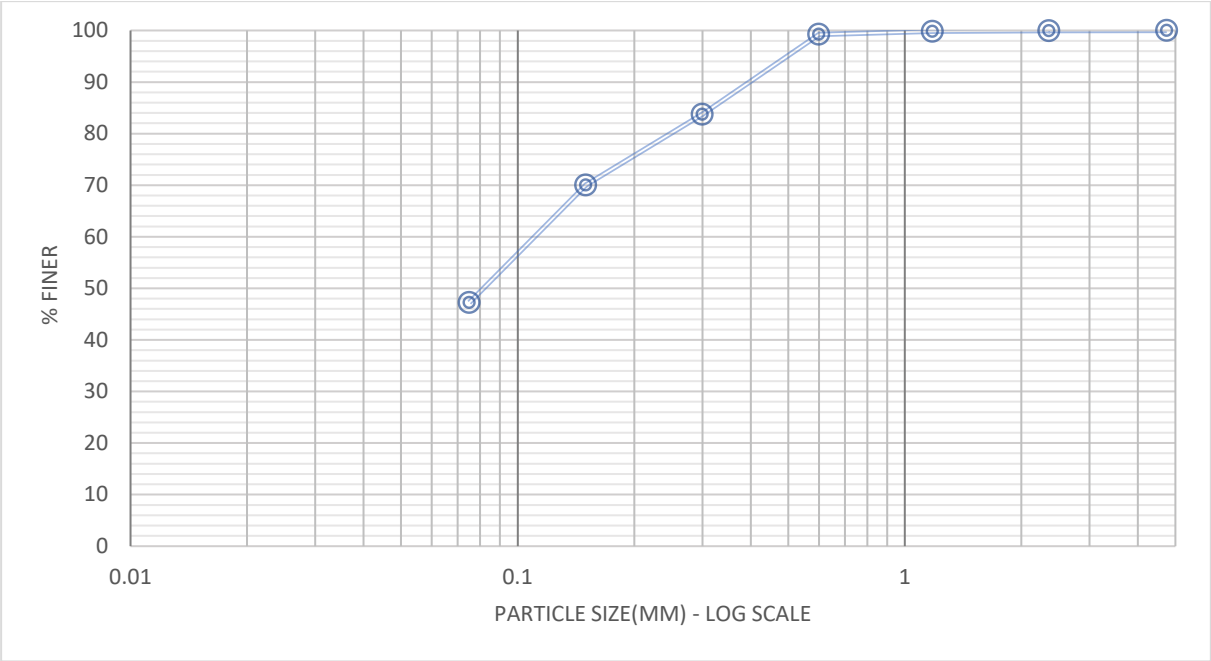

Table 3-8 Grain size distribution for depth of 1.83-1.95 m and 2.15-2.27 m

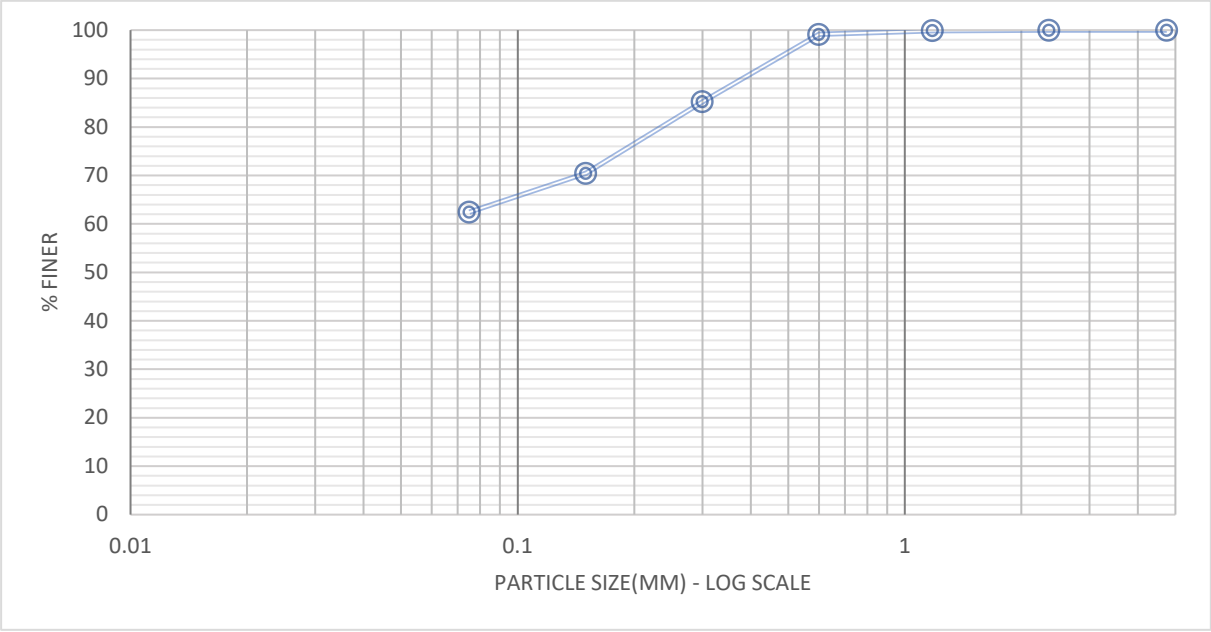

Table 3-9 Grain size distribution for depth of 2.56-2.70 m

Grain size partitions (less than 0.075mm) are off the plots due to the hydrometer tests that probably had wrong input values in regard to the formula which is used for calculating the grain sizes. In the results, the sizes of the grain sizes of the partitions is very small (29% of the grains are <0.0001mm, and approximatively 13% of the grains are <0.00001mm), which doesn't fit the grain size distribution of any soils as the grains are too small in size. Considering that, the hydrometer test distribution will not be plotted.

Soil Classification

Therefore, the soil will be classified according to the following standards:

A. Unified Soil Classification System (USCS) (Budhu, 2010)

Following the flowchart classifications (coarse-grained or fine-grained soils) soil is either SC (Clayey sands, sand-clay mixtures) or SM (Silty sands, sand-silt mixtures) with sand content of up to 53% and clay and silt content of 47% (less than 0.075mm). Considering the plasticity chart where the L.L. = 18.39% and P.I. = 2.69%, soil is classified as SM – Atterberg limits below “A” line or hatched zone and P.I. < 4%.

B. American Society for Testing Materials Classification System (ASTM-CS) (Budhu, 2010)

ASTM-CS presents another system of classification where soils cand classified by group symbols and group names. The current specimen is therefore classified as Silty Sand (with fines of ML or MH) or Silty, clayey sand (with fines of CL-ML), according to the flowcharts for coarse-grained or organic/inorganic fine-grained soils.

C. Indian Standard Soil Classification System (ISSCS) (Ranjan and Rao, 2007)

According to the ISSCS, the soil is classified as SM (Silty sands, sand-silt mixtures), with P.I. below “A” line or hatched zone.

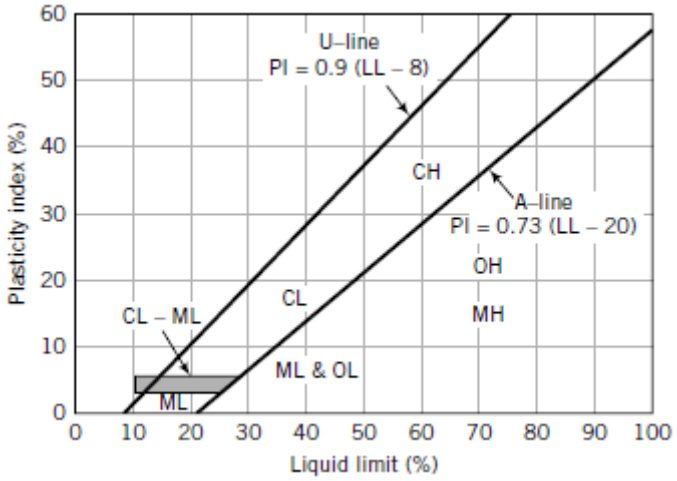

Figure 3.10 Plasticity chart reproduced from (Budhu, 2010)

Chapter 4: Case study – Sjoskrenten

4.1. Site description

The case study represents the study of the pile foundations for a construction and rehabilitation project, that is planned to be finished and given under exploitation in the autumn of 2022 to February 2023, according to the local sources ((Bårdseth, 2020) and (Jonassen, 2021)) . For the thesis purposes, the main stakeholders are presented as Store Norske Spitsbergen Kulkompani (SNSK) that will build the new buildings for Svalbard Folkehøgskole, and Hæhre Arctic that has won the tender competition (Byggebransje, 2021). Multiconsult Company will provide the foundation planning (PELEPLAN) for the current project (see Figure A.4 for a general overview). As it can be seen in Figure 4.1, the extension of the campus will be done around an existing building that was used as a dormitory for the UNIS students, that belonged to the UiT Arctic Students' Organization. Figure 4.1 (a) was edited from a situational plan done by LINK ARKITEKTUR, for the purposes of showing the existing and under construction infrastructure. The sensitive information and dimensions on the edited figure were covered and colored, for the copyright purposes.

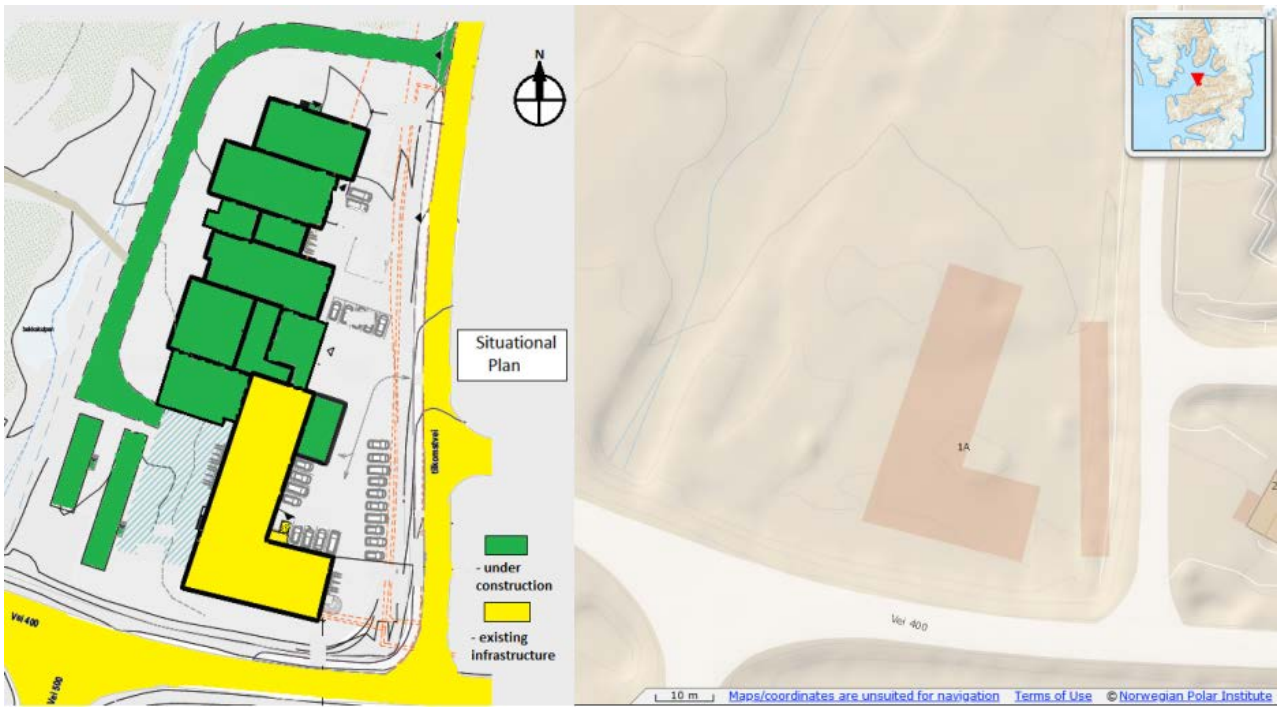

Figure 4.1 Site overview: left (a) – situational plan; right (b) – general location of the existing infrastructure (Norwegian Polar Insitute, n.d.)

For the current investigation, I was present at the ground drilling and pile driving, located in the vicinity of the existing infrastructure. Steel piles were driven manually with a crawler excavator by use of a grapple claw in a 10m borehole depth (see Figure A.**5**). On a weekly basis, the ready-mix concrete was poured into the well on the first 8 meters, that is up to 2 meters below the ground level. Cross section of the pile foundation is presented below:

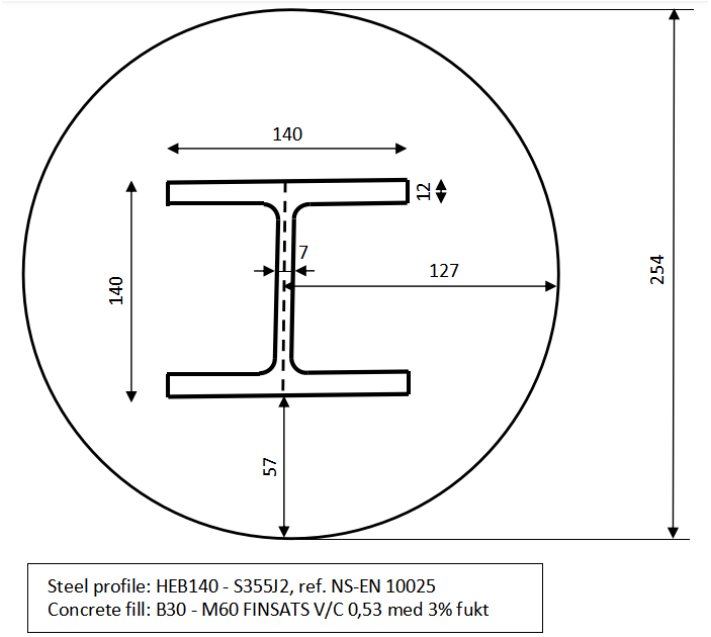

Figure 4.2 Cross section of the well and steel profile

4.1.1.Temperature regime

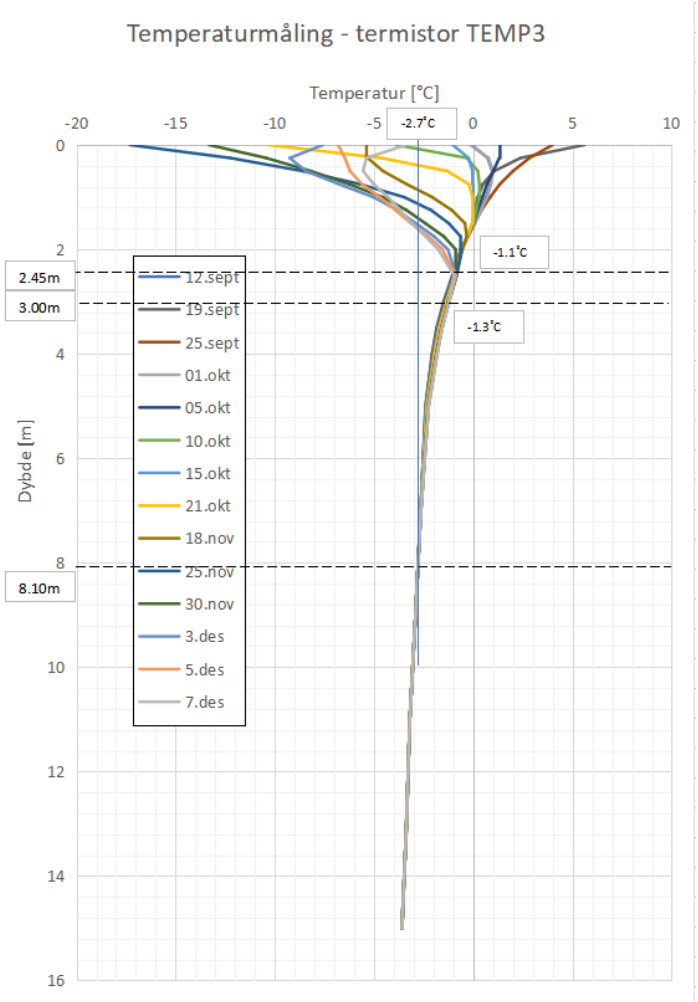

Figure 4.3 Trumpet curves of the local ground

Figure 4.3 shows the thermal state of the ground of the AOI, done by Multiconsult. Depth of zero annual amplitude (ZAA) is located at 2.45 m. The other 2 marked distances with their specific temperatures will be discussed further on in the thermal measurements with the thermocouples and thermistors. According to the short-term observed data, permafrost starts at a depth of approximative 1.5m below the ground.

4.1.2.Soil classification according to the local stakeholders

After the thorough geotechnical investigations, the results were found as shown in the Table 4-1 and Figure 4.4. The soil represents mainly the silty clayey type of soil (less than 25% of the grains correspond to clay dimensions), with an average water content of 23.24% and salinity of 25.0 ‰. Salinity values are relatively larger than for the UNIS East specimens that constitute of up to 2.1 %. Generally, silt is mainly predominant (up to 45% of the grains), with high amounts of fine sand and partly gravel.

SYMBOL	DEPTH(m)	Description	W (%)	Salinity (‰)	Undrained shear strength (kPa)
A	2.0-3.0	SILT, clayey, sandy	25.4	N/A	2.0
B	3.0-4.0	SILT, clayey, sandy	24.0	N/A	3.5
C	4.0-5.0	SILT, clayey, sandy	22.1	N/A	11.5
D	5.0-6.0	SILT, clayey, sandy	24.3	25.0	4.5
E	6.0-7.0	SILT, clayey, sandy	20.4	25.0	10.0

Table 4-1 Soil description and characteristics

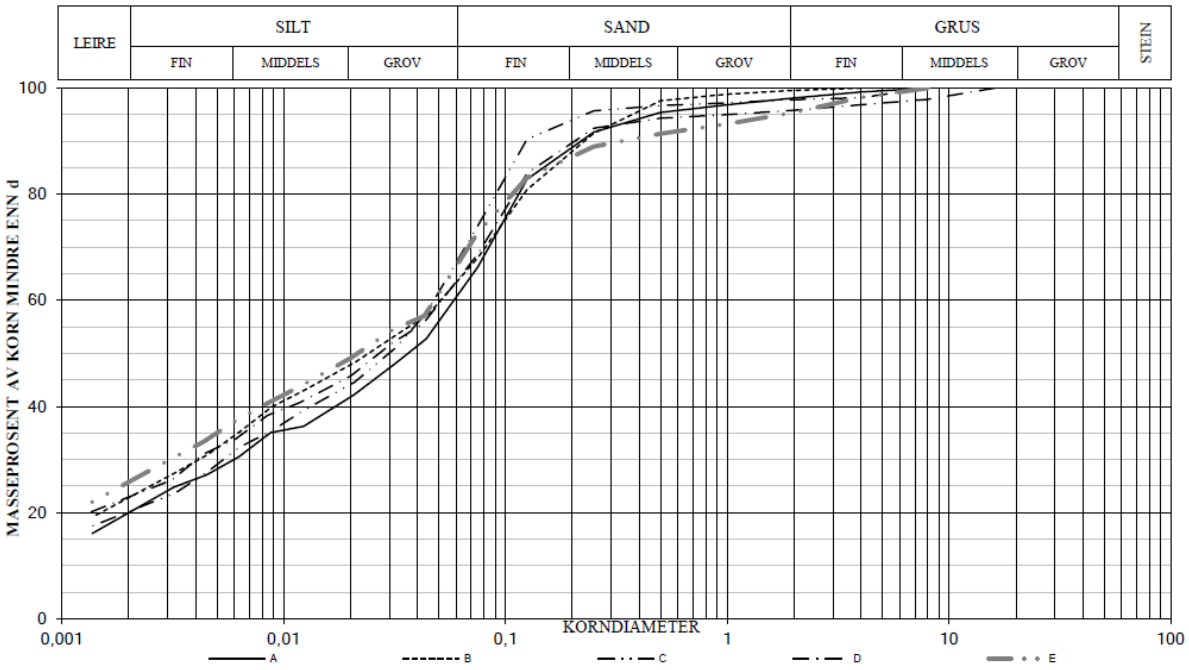

Figure 4.4 Grain size distribution for the characterized samples

Soil analysis has been done in October-November 2021 under the Store Norske Spitsbergen Kulkompani AS direction for the Svalbard folkehøgskole project by Multiconsult and LNSS. It is of a tremendous importance to mention that during the supplementary ground surveys, in most of the tested boreholes at depths of 1.0-2.0m, significant water infiltration was found.

4.2. Thermal measurements

Thermal measurements were done on behalf of the piles that were driven to the immediate position of the existing building 1A (see Figure 4.1(b) for the existing building 1A, Figure A.5 and Figure A.10 for a general picture).

4.2.1.Thermocouple measurements

Generally, thermocouple measurements were done in two phases on the site, and one trial in the laboratory conditions which will be described in the current chapter.

Mechanism of functioning consists of a sensor composed by two wires, with a dissimilar type of metals for both wires. One wire end responds for the temperature measuring while the other for the reference junction that is connected to the logger. By correlating the obtained voltage to the temperature, logger retrieves the converted output. For the thermocouple measurement, we opted for the Comark N2014 Data Logger Type K, that uses the EV Software to program the logger and to examine data after the logging. It operates at -200°C to +1372°C with an accuracy of ±0.5°C +0.5% (±0.9°F +0.5%) of reading over the range of -80°C to thermocouple limit (see Figure A.11 for details). For this logger, up to 3 external point sensors can be connected, excluding the built-in temperature sensor.

The procedures for preparing the cables and input data involve a more comprehensive solution, but somehow similar to the recommendations made by Norwegian Public Roads Administration (NPRA, 1996). The setup of the first measurement consists of 2 points located at the same depth (8.10m below ground) - one point close to the pile, another to the permafrost (see Figure 4.5). Data log started on 16/02/2022 12:01 PM and ended on 23/02/2022 12:01 PM, with a logging interval of 30 minutes. Temperature of concrete at pouring was 4.5 ˚C, which started at 01:38 P.M. (13:38) on 02/16/2022.

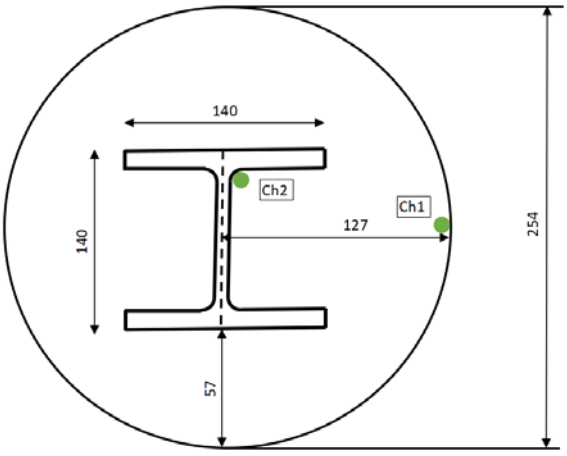

Figure 4.5 Location of the thermocouples

Ch1 represents the destination close to the well wall, while Ch2 is located on the steel pile. The Ch2 cable was installed after the pile was heated with a Gas Torch, otherwise the tape holding the wire would not stick to the steel pile.

Retrieved data can be observed in Figure 4.6 that is a temperature evolution for the 14 hours of recording. Ch1 and Ch2 are defined by similar trends and overlap. Ch4 responds for the built-in sensor, respectively the air temperature above the ground. A spike in temperature can be observed at 1:55 P.M., after the concrete was poured, with a general trend stabilizing at -2.8 ˚C (Ch1) and -2.6 ˚C (Ch2) at the end of 7 days of logging (see Figure A.8 for full data). For a general comparison, permafrost at depth of 8.1m below ground has a temperature of -2.7 ˚C (see Figure 4.3).

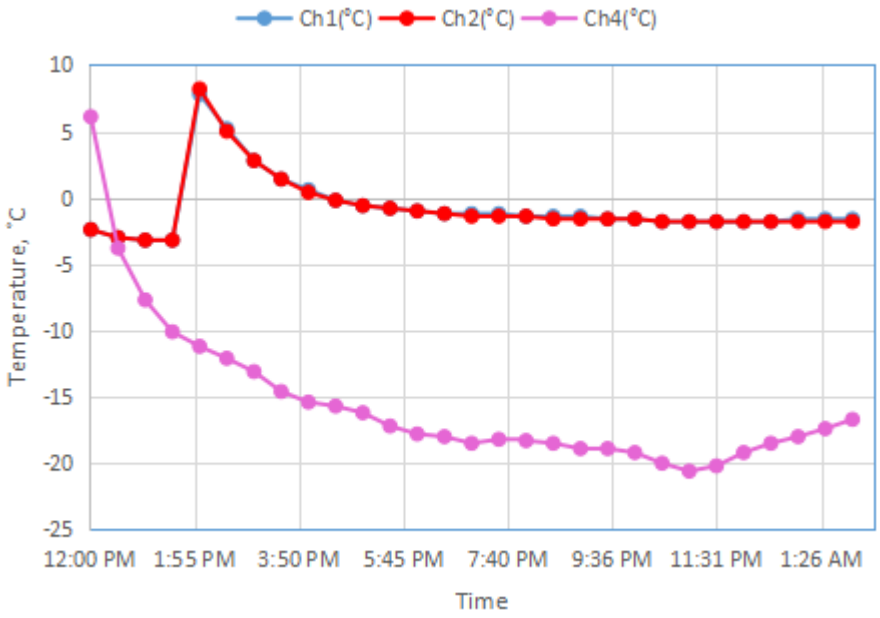

Figure 4.6 Temperature data Meas.1 – first 14 hours of measurements

From the Figure A.8 general futures can be observed:

- To mention is the temperature of the Ch1 and Ch2, respectively 7.8 ˚C and 8.2 ˚C at 14:01 P.M. The difference between the registered temperature and that of the concrete at pouring (4.5 ˚C) speaks about the cement hydration that leads to an exothermic reaction. Concrete pouring started at 1:38 P.M.

- Concrete is having a temperature below the 0.0 ˚C after 4.5h from first log, respectively at 16:31h, or approximatively 3h after pouring.

- For the Ch4 data, spikes in the temperature can be observed because warm pads were used on the logger surface in order to not to drain its battery as the temperatures were lower than -20 ˚C.

- Initially, Ch2 seems to lose heat faster than Ch1, respectively transferred via conduction through the steel profile until the 1.5th day after pouring. After a certain period when heat of hydration is lower, Ch1 tends to achieve the thermal equilibrium with the permafrost at a higher rate. Temperature data for Ch1, that is located near the borehole wall, shows lower values than for Ch2,

by a range of 0.2 to 0.4 ˚C, starting with approximatively the 5th day after pouring of concrete until the end of logging.

The setup of the second measurements consists of a combination of thermocouple and thermistor measurements. For the thermocouple, there was 1 point located at an approximative depth of 3.00m below ground level, in an aleatoric location, not connected to the steel pile. There is a possibility that the cable was not fully stretched, therefore the approximation of depth was done. Data log started on 16/03/2022 07:00 A.M. and ended on 23/03/2022 with a logging interval of 20 minutes, for more accuracy. Concrete was poured on 16/03/2022 at 02:29 P.M. (14:29).

The output of the measurement can be observed in Figure 4.7 that represents a thermal evolution for the 14 hours of recording, after 12:00 P.M. Ch1 depicts the point sensor, while Ch4 responds for the built-in sensor, respectively the air temperature above the ground. Similarly with the Measurements no.1, an increase in temperature can be observed at 02:40 P.M. (14:40) to 5.6 ˚C, after the concrete pouring, with a lowering trend that is stabilizing at -4.6 ˚C at the end of 7 days of logging (Figure A.9 shows the data for 7 days). Temperature below 0 ˚C was achieved 2 hours after the pouring of concrete. Generally, permafrost at depth of 3.0m below ground has a temperature of -1.3 ˚C (see Figure 4.3). The difference between the temperature that the logger sensed (a down trend to -4.6 ˚C after 7 days) versus the permafrost temperature at that depth must be because of lack of permafrost and/or water infiltrations. Otherwise, the thermal regime of that specific area is different from the borehole that is described in Figure 4.3 even though both the wells are located at a relatively close distance (5-10m).

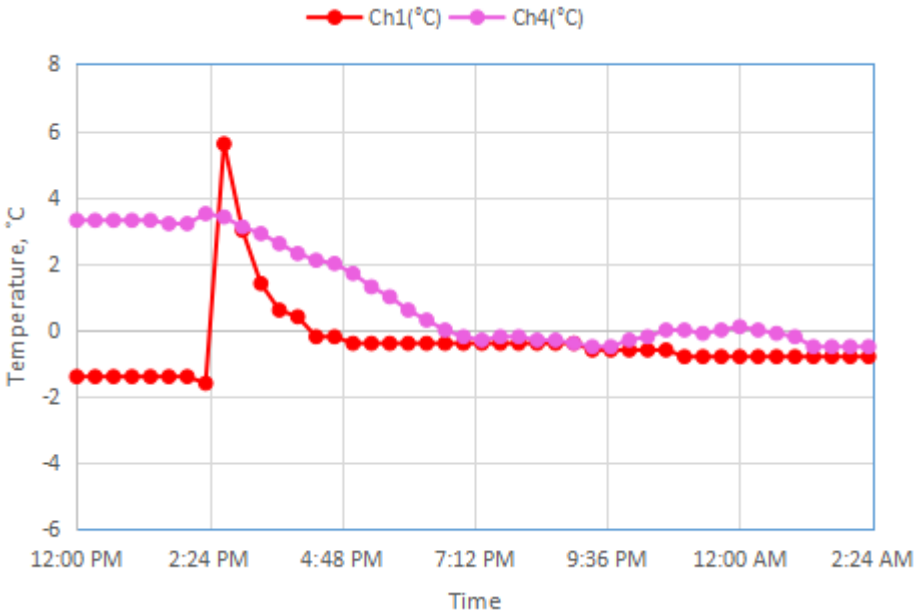

Figure 4.7 Temperature data Meas.2 – first 14 hours after 12:00 P.M.

The rise in temperature for the Measurements no.2 is not as similar as for the Measurement no.1, even though a higher temperature of the air for the second measurements should give a relatively larger hydration heat. Peak temperature was received on 16/03 at 02:40 P.M. (14:40), that resulted in 5.6 ˚C. Two hours after the pouring of concrete, the temperature went below 0.0 ˚C with a down trend.

4.2.2.Thermistor measurements

The logging of the thermistors happened on the same period as for the 2nd measurements with the thermocouples, at the same depth of 2.80 to 3.00m below ground, and at the same pile. Position was aleatoric as long as it's located in the cement slurry, but not close to the steel section.

The UNIS thermistors and logger function a bit differently from the thermocouples, where the installation of the wires is slightly easier, and the temperature data comes directly converted as an output. For the output data, the CR1000X Campbell measurement and control data logger was used which operates in a range of -40° to +70°C. Its wiring panel includes two switchable 12 V terminals, analog grounds dispersed among 16 analog terminals, and unpluggable terminal blocks for quick deployment (Campbell, n.d.).

An excitation channel VX3 (sending a specific voltage at a specific time to excite the resistance) and an analog SE channel 7H (single ended, measuring the voltage sensing that comes back) was enough for the setup of the connection with the logger (see also Figure A.12 for a general overview). The wire end was covered with silicon glue for any humidity to be expelled. The measurement took place at a depth of 2.80-3.00m approximatively. Logging initiated at 07:00 A.M. 16/03/2022, until 23/03/2022 at 12:01 P.M. with a time step of every 5 minutes. Concrete was poured on 16/03/2022 at 02:29 P.M. (14:29).

The output of the first 14 hours after 12:00 P.M. are showed on Figure 4.8. T2 represents the sensor that recorded the voltage which is converted to temperature data. An increase in temperature can be observed immediately after the pouring of concrete, at time step between 14:20 and 14:30 with the peak temperature achieved at 14:30, as 9.93 ˚C, with a trend lowering towards -5.5 ˚C at the end of 7 days of logging (see Figure A.13 for the output of the 7 days). Temperature below 0 ˚C was achieved exactly 1 hours after the concrete pouring. Generally, permafrost at depth of 3.0m below ground has a temperature of -1.3 ˚C (see Figure 4.3). The same as for the thermocouple data, the difference between the temperature that the logger sensed (a down trend to -5.5 ˚C after 7 days of logging) versus the permafrost temperature at that depth must be because of lack of permafrost and/or water infiltrations. Otherwise, as has been said the thermal regime of that specific area is different from the borehole that is described in Figure 4.3 even though both the wells are located at a relatively close distance (5-10m).

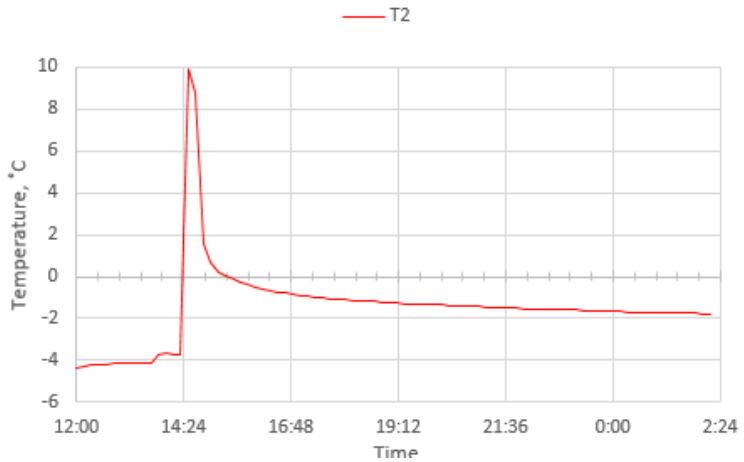

Figure 4.8 Thermal development for the first 14h after 12:00 P.M. Thermistor channel T2

4.2.3.Hett97 Norcem Simulation

In order to compare with the obtained data in regard to the thermal development, a simulation was created, by using the Hett97 Norcem Simulation. Simulation was done for the 8.1m depth below ground temperature regime, thus comparable to the first thermocouple measurements. The tool is developed by Norcem Heidelberg Cement Group and represents a planning software that simulates the temperature and strength development of a concrete structure in the post-cast state (Fredvik, n.d.). The input data is generally related to the type of formwork, concrete section type and dimensioning, concrete specifications (incl. additives), heating options, temperature and wind data, and time (see Table 4-2 for the input). Simulation was done for 7 days, equal to 196h.

Section type	Column, circular
Radius	12.5 cm
Concrete specifications	STD B30-M60 uten P-stoff
Real specifications*	STD B30-M60 with additives: 1.5 % Mapefast SA
Concrete temperature	4.5 ˚C
Air temperature = permafrost	Constant: -2.7 ˚C
Wind Strength	Still - No wind
Formwork type**	Steel 3mm, not isolated
Formwork removal	1h
Cement + Silika density	394 kg/m3
28-days compressive strength	47.5 Mpa
Extra heating***	Heating cable 16W/m
Radius of heating cable	0.001m
Number of heat cables	00000
Removing of cable	1h

Table 4-2 Input data Hett 97

*According to the specifications of the concrete, the additives were corresponding to the 1.5% Mapefast set accelerator (see Figure A.7 for the densities of the compounds). The closest option for the input in the software was STD B30-M60 without P-stoff.

**It was not possible to exclude totally the formwork, therefore I used the steel 3mm, as it will transport heat faster than any formworks that were listed. This case is the more representative scenario. Formwork removal after 1 hour (minimum required by the software).

***It was not possible to select 0 W/m, however the number of heating cables was selected as 0, which gave an input of “Not in use” for the heating. Also, the heating cable was removed after 1 hour (minimum required by the software).

The output will be shown as follows:

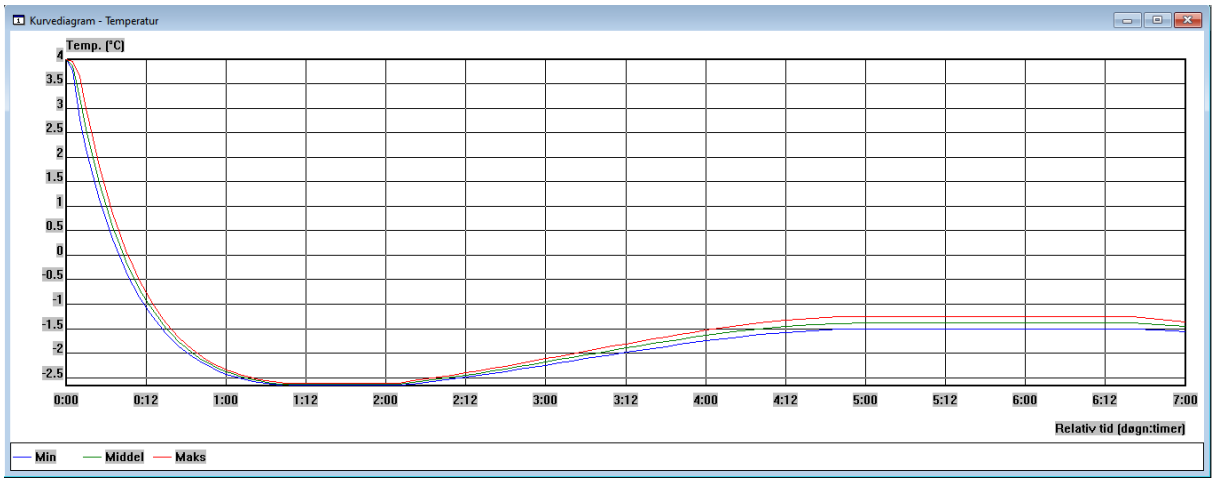

Figure 4.9 Temperature development for the 7 day of simulation

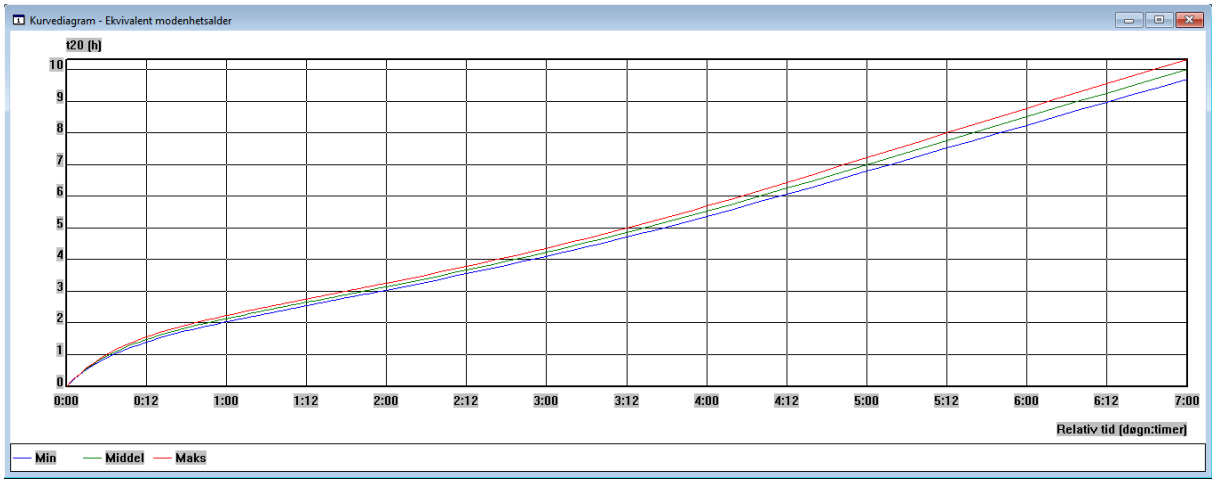

Figure 4.10 Equivalent maturity age

Several observations can be made on basis of the output from the heat development simulation:

- Minimum, Medium, and Maximum are related to the regions in the concrete section. The center of the pile section is respectively losing the less heat, while the edge is having a larger heat transfer with the permafrost.
- According to the simulation (see also Figure 4.9), concrete is entering the below 0°C after 7-9 hours (NO.: Tid for frysing). The time is merely larger as compared to what measurements show, for reasons such as: simulation takes into account the full concrete pillar (no embedded steel profile considered), formwork consideration for 1h, and probably the heating input for 1h. Therefore, the results could be a bit exaggerated, as speaking about the equivalent maturity age of the concrete.
- An equivalent maturity age (M) of the concrete expressed in t_{20} hours, resulted in values of 9.7 to 10.3 hours after 7 days, depending on the location in the section of the concrete (see Figure 4.10 and Figure A.18 for a distribution over the concrete section). To remind, the reference temperature in the equivalent age is 20 °C.

- Concrete compressive strength after 7 days and after 28 days of cast are showed in Figure A.15 and Figure A.16. After 28 days of pouring, concrete is achieving barely 22.0 Mpa, which is considerably lower than the reference compressive strength of the current concrete: 47.5 Mpa.

4.2.4.Lab Thermal regime (thermocouples)

With the LNSS help with concrete supply, the concrete hydration temperature was measured in the lab UNIS conditions for 3 different temperature regimes, respectively 16˚C (room temperature - Ch1), -3 ˚C (an equivalent for the temperature of permafrost – Ch2), and -18 ˚C (simulating the freezing of the concrete – Ch3), for a period of 10 days. Logger was placed in the same location as the Ch1 that was measuring the concrete left at 16˚C. Thermocouple end was placed directly in the concrete tara/vessel.

For the Ch1 and Ch2, no visible hydration heat release is observed for the first 14 hours (see Figure 4.11). Ch1 shows a dependency with the room temperature (Ch4), while Ch3 reaches the below 0 ˚C in less than 1 hour. The 10 days period can be observed in Figure A.19. Moreover, cyclical deviations in temperature can be noticed on the plot due to the heating system changes.

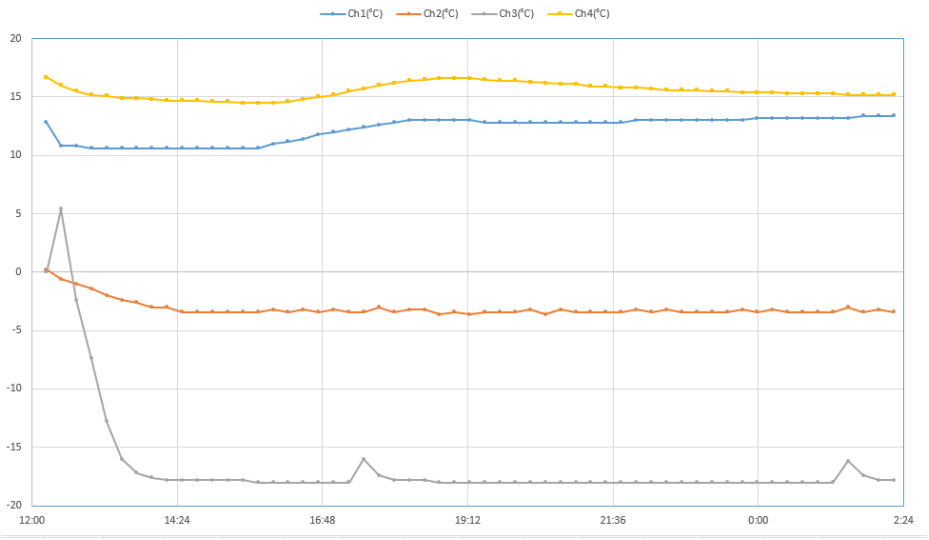

Figure 4.11 Thermal regime of the tested samples, Ch4 represents the logger temperature

Another setup of a simulation represents almost the same specifications as in Table 4-2, but with changes in order to obtain the reference concrete behavior of 20 °C: concrete temperature = 20 ˚C, air temperature = constant, 20 ˚C, respectively:

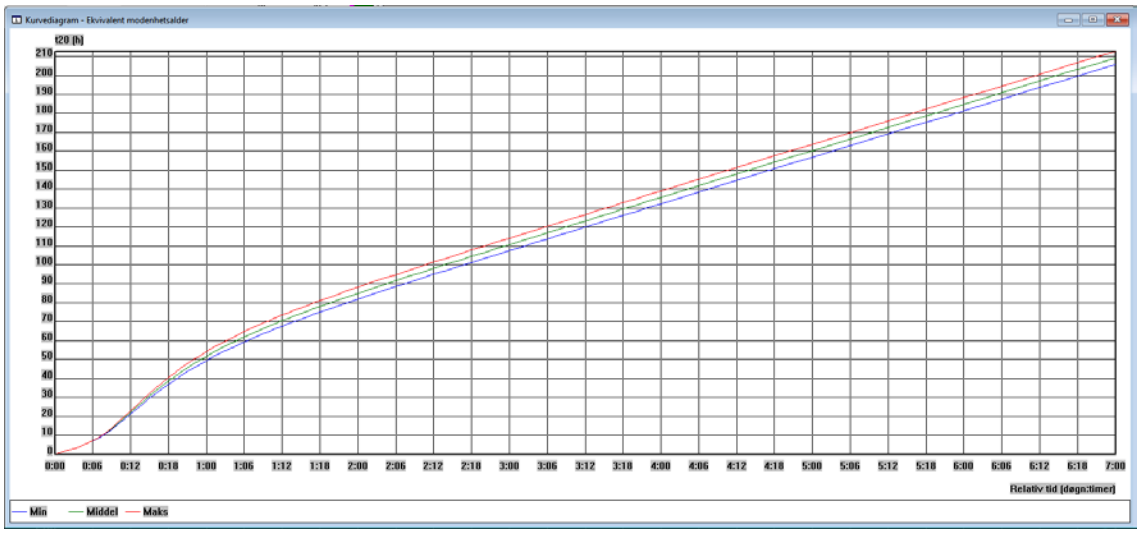

Figure 4.12 Equivalent maturity age of the 20 ˚C reference concrete

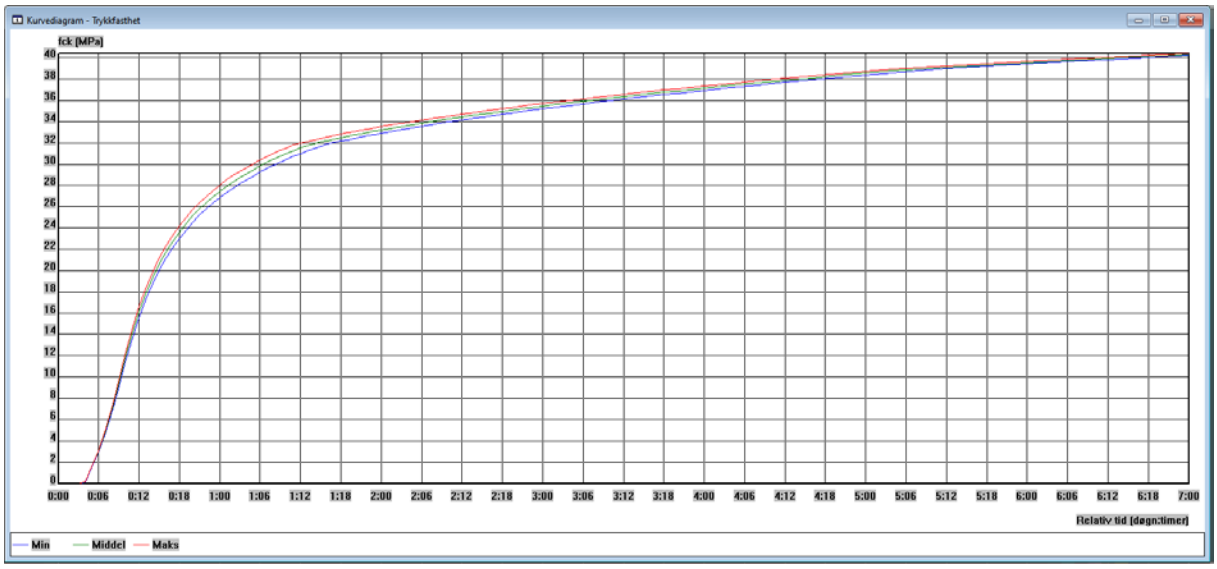

Figure 4.13 Compressive strength development at reference 20 ˚C for 7 days

Quantitatively, the equivalent maturity age of the concrete cured at -2.7 °C after 7 days is at a low value as compared to the same concrete that could develop at 20 ˚C (see Figure 4.12). For the compressive strength, the time of development is twice faster for the 20 ˚C as for the concrete cured at -2.7 °C.

4.3. Adfreeze strength and shear tests

Adfreeze strength tests were done in two stages on four different concrete samples. Concrete samples were cast in plastic cylinders at different temperatures, and have the following characteristics (Figure A.20 shows the preparation stage):

No.	Concrete B30 dimensions: Diameter x Height, [mm]	Sample characteristics
#1	57 x 88	concrete was cured at room temperature, 16˚C

#2	56 x 75	concrete was cured at permafrost temperature of -3 ˚C, and w/c is lower than #3
#3	57 x 85	concrete was cured at permafrost temperature of -3 ˚C, and w/c is higher than #2
#4	56 x 81	concrete was cured at -18 degrees

Table 4-3 Concrete samples specifications

As the concrete samples are relatively small in volume and size, there is a higher probability that w/c ratio may vary, due to the concrete pouring (the more liquid paste is flowing faster than the denser one). After a number of 10 days, the plastic formwork cylinder was cut with a circular saw in the laboratory conditions.

4.3.1.Samples preparation

The setup was prepared with the soil extracted from the UNIS EAST location. Four buckets were prepared for 2 different stages of adfreeze shear tests. For the tests, the silty clay soil was compacted at a water content of 23.24%, that represents an average of the water content in the soil that was examined on the Svalbard Folkehøgskole project by Multiconsult company.

Initially, a hole of 8 cm diameter was cut with the manual saw on each of the buckets, or relatively 2-3 more cm than the concrete sample diameter. In order to reproduce the shear movement in the soil, the concrete cylinder (resembling a concrete pile) was inserted in the prepared bucked immediately after the 10-day post cast process, in the middle of the 8 cm hole location. Afterwards, the soil was inserted up to the exact height of the concrete cylinder. During the pouring process, soil was manually and gradually compacted with the spatula and shovel (Figure A.21 shows the preparation stage). According to recommendations, vacuum should be applied on top of the soil sample, while water is supplied at the base (Ladanyi and Theriault, 2008). Moreover, in order to keep an unidirectional freezing of the process – for an uniform distribution of the water content and ice lenses, lateral insulation is suggested to be used (Ladanyi and Theriault, 2008) and (J. S. Weaver and Morgenstern, 1981). Due to lack of resources, the soil was not isolated thermally or vacuumed. However, for keeping a constant water content in the soil samples, buckets were wrapped in plastic film. All the samples were stored in the cold lab room at a temperature of -3 ˚C.

4.3.2.Description of the apparatus

For the current tests we used the Knekkis uniaxial compression machine, located in the UNIS cold laboratory (Figure A.22). It consists of two plates situated at a modifiable distance one from another. The sample is loaded from below (bottom piston) while the top plate of the Knekkis is in a fixed position. The pressure is recorder by the upper plate with a load cell.

A relatively simple custom-made setup was used for the adfreeze shear strength determination. It consists of a concrete cylinder that is placed in a prepared soil environment (Figure 4.14). By applying a uniaxial force (from the down piston of the Knekkis machine) with a specified rate, we obtain an elongation or movement of the concrete sample along the soil surface. The connection between the concrete sample and

the upper arm of the Knekkis is done through a steel cylinder support. Dimensions of tools are also presented in Figure 4.15.

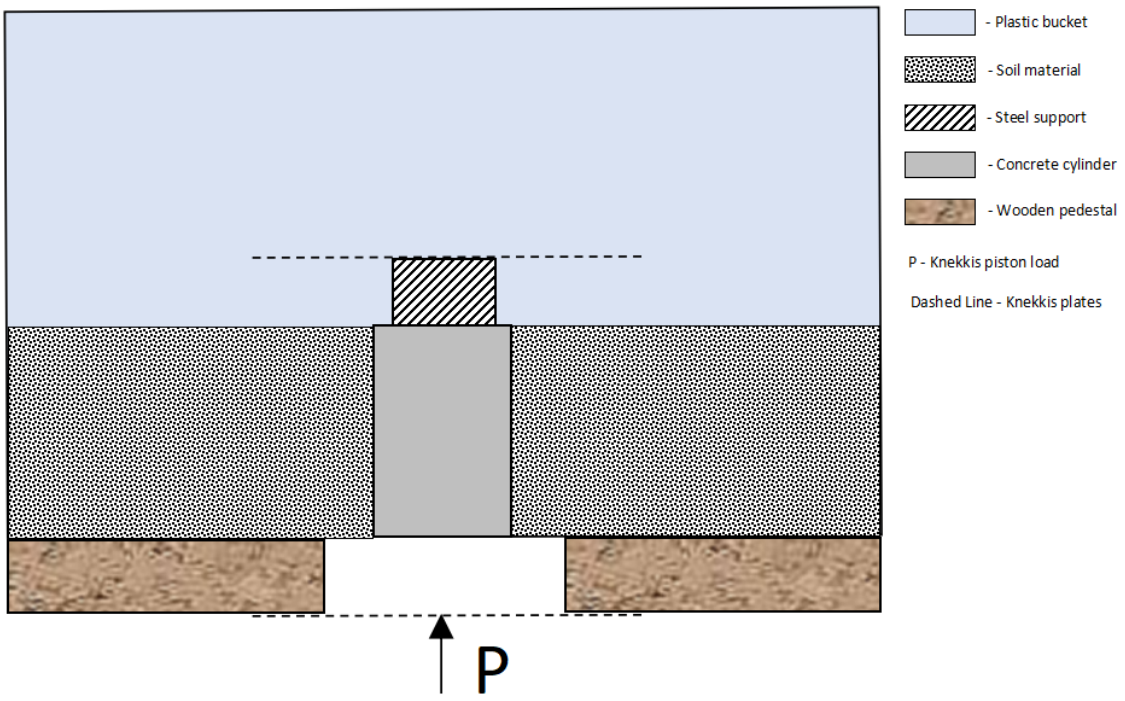

Figure 4.14 Adfreeze strength setup

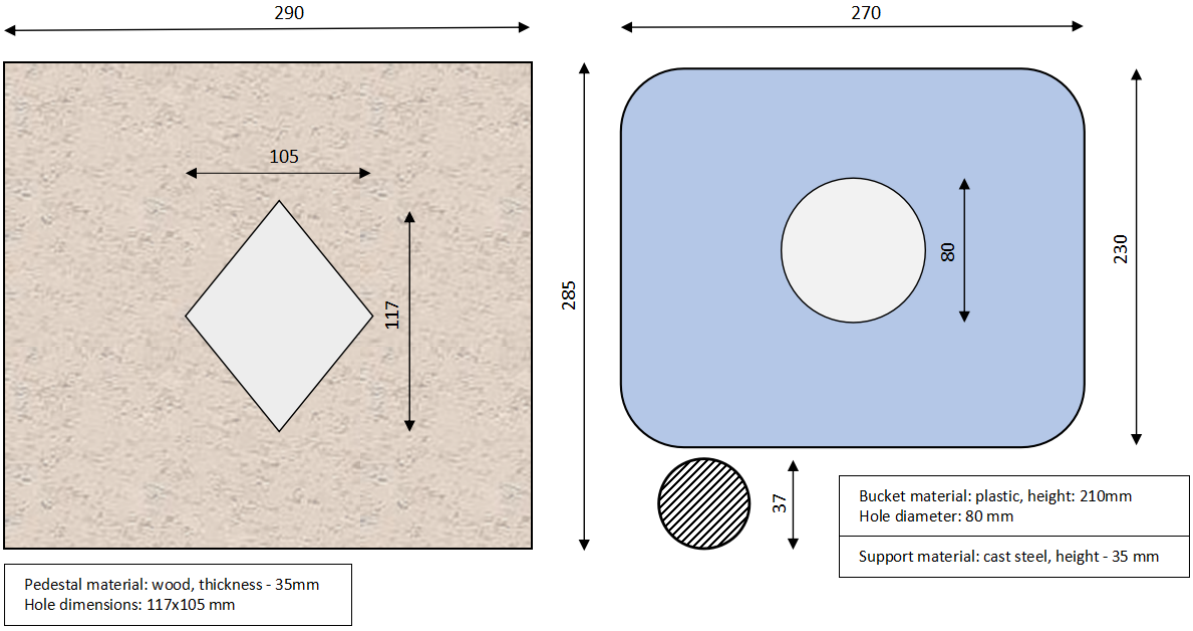

Figure 4.15 Used tools dimensions: left – wooden pedestal, bottom right – steel support, right top – plastic bucket

4.3.3.Adfreeze Shear testing

The current setup for the Knekkis device was used:

- Deformation rate of 0.01%/min (from height of the concrete cylinder).

- Autostop of the pressure force after 30 mm.

- Maximum allowed load of 90 kN.

- Dimensions of the concrete cylinder and temperature data was inserted manually.

Adfreeze shear strength is deducted from the Passive shaft adfreeze force (Adfreeze bond) formula as described (Andersland et al., 2003):

$$P_p = 2\pi a \sum_{0}^{L_p} \tau_{ai} \Delta L_i \tag{21}$$

Where $2\pi a$ represents the perimeter of the pile shaft for a circular pile, τ_{ai} is the relevant shear resistance (or adfreeze bond) for a layer *i* with thickness ΔL_i, and L_p is the embeded pile length.

Strain will be determined as follows:

$$\varepsilon = \frac{\Delta L}{L_0} \tag{22}$$

Where ΔL is the Elongation and L_0 presents the original length.

4.3.4.Results

Stage 1

At the current stage, the short-term adfreeze shear strength was determined. It is important to mention that during 3 days before testing, the four soil sample buckets were kept in the cold laboratory where the Knekkis device is located, due to lack of space in the initial cold laboratory. The deviation of the temperature in the Knekkis laboratory is relatively high (see also Figure A.22b), therefore it was not possible to keep it constant. The temperature of the soil had to be constant, in order to resemble the permafrost conditions on the Svalbard Folkehøgskole project, that is approximatively -3 ˚C at 8.1 m below the ground level. Even though the temperature was established as -3 ˚C, we encountered moments when it presented as low as -18 ˚C. Results of the short term adfreeze strength for all the four case studies can be observed in the following figures:

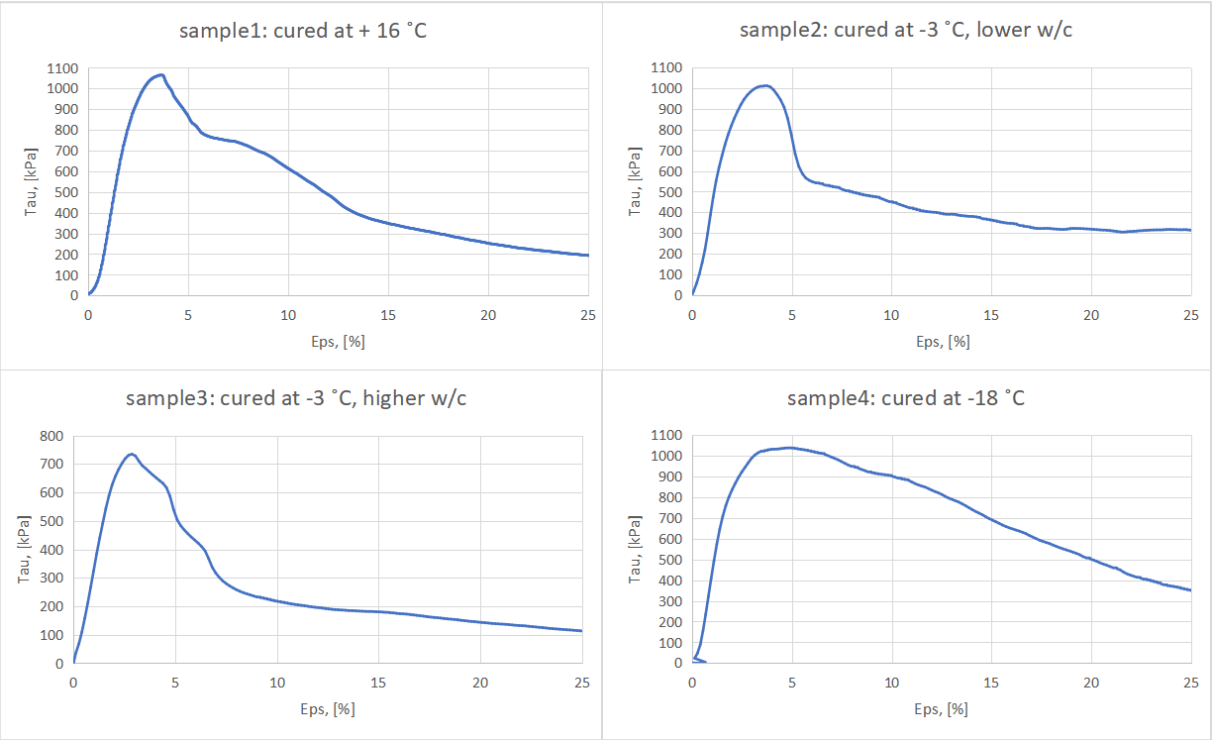

Figure 4.16 Stage 1 Shear - Strain results for all the four case studies

A general failure mechanism along the soil depth is observed on all of the soil samples, for example Figure A.23 shows the visible displacement surface along the well depth for the sample #1. The failure mechanism represents the dilatant behavior with strain softening. Peak strength occurred at a displacement of 2.5 to 4 mm, or in the first 3 to 4 minutes of the testing but the tests were continued up until 30mm. It is expected to have a higher adfreeze bond strength when the temperature in the soil lowers down, also observed in the Frozen Ground Engineering book (Andersland et al., 2003). Therefore, for this stage the values may be exaggerated if compared to the literature, as the temperature of storage room before testing was down to -18˚C. For example, it is described that peak values for the ice-rich silt's Adfreeze Strength on steel piles represent up to 250kPa, while for the stage 1 tests we encountered a higher degree of bonding between the soil-concrete model (1064 kPa for the sample#1 and 1039 kPa for the sample #4). Moreover for the sandy soils in contact with the concrete piles, the adfreeze strength is differing, respectively with given values of up to 320 kPa at -4˚C (J S Weaver and Morgenstern, 1981). It is also expected that concrete piles will develop a slightly higher adfreeze bond strength than the steel piles, due to difference in the surface roughness (Parameswaran, 1980). Furthermore adhesion strength of ice to concrete pile surfaces are reported from 400kPa to 1117 kPa , which could correspond to highly ice-saturated soil (Barker et al., 2021).

Stage 2

After 1 day of warming and thawing at room temperature, and after 2 days of freezing at -3 ˚C in the cold laboratory, the tests were done one more time in order to observe a residual bond healing process. During the stage 2, the temperature of the samples was kept at a constant value of -3 ˚C while stored and tested. The water content remained the same, 23.24%, as the samples were wrapped totally in plastic film. In the bond healing tests, the shearing test is resumed after a period of time, under the normal

pressure (Ladanyi and Theriault, 2008). A recovery in the adfreeze shear strength can be observed in the following figure:

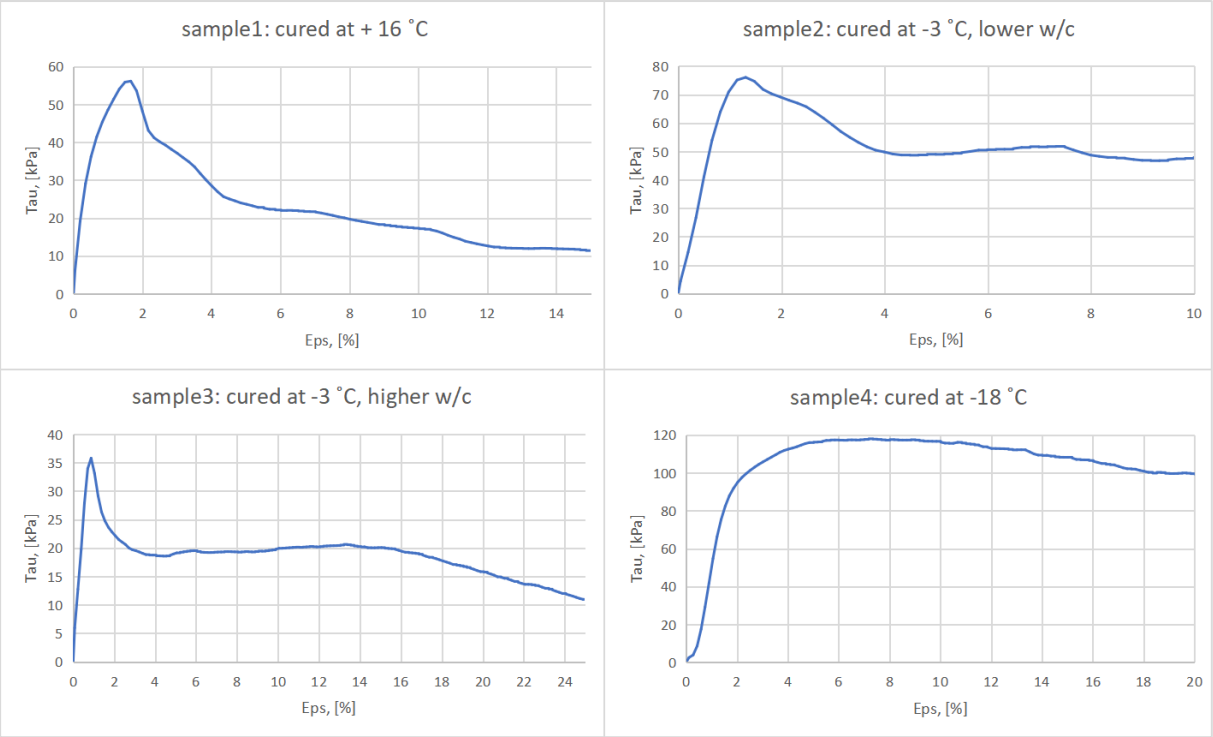

Figure 4.17 Stage 2 Shear - Strain results for all the four case studies

A clear bond with time is observed on top. It could be, that in time a complete recovery is expected (Ladanyi and Theriault, 2008). It is interesting to observe that the recovery for the sample 4 is twice the value of the sample 1, even though the peak strength values were close (Ladanyi and Theriault, 1990). It is mainly considered that recovery, or the bond healing is highly dependent on the unfrozen water content of the soil, therefore for the sample 4 (that has a higher UWC due to a lower curing temperature of the concrete) the recovery happens with a faster rate. The reason could be attributed to the fact that sample 4 used less bound water for the hydration process as it got frozen at a faster rate, and therefore the interface between soil-concrete, and probably the close to it soil material, had a higher UWC.

It is important to mention that after the stage 1 tests, concrete samples were not deformed as the applied compression force was considerably lower than the maximum compression resistance of the B30 concrete. Knowing that surface roughness is a factor in influencing the adfreeze strength, it should have the same degree of influence in both of the test stages, as concrete samples were the same specimens (e.g. roughness of the stage1 sample#1 is relatively similar to roughness of the stage2 sample#1).

After thawing of the soil and looking on all 4 of the concrete samples, it is observed that the first three are having a smooth lateral surface, while sample #4 is more rigorous/jagged. Figure A.24 shows all four of the tested samples, while in Figure A.25 close observation of the sample #4 is visible. The coarse roughness of the concrete surface may be due to the increased soil-concrete bond because of a higher unbound water content in the concrete sample, that did not participate in the hydration process.

Chapter 5: Discussion

5.1. Adfreeze shear strength

According to Andersland and many other findings in relation to the shear behavior of frozen sands, the four mechanisms that govern it are pore ice strength, soil strength, adhesive ice bond, and mutual strengthening effects between the soil and ice matrix (Andersland et al., 2003). In addition to the mechanisms above, the density of the soil, temperature, confining pressure, and deformation history will have a significant importance, as well. Specifically for the Longyearbyen future regarding climate change, while the soil remains ice-rich enough for binding of the grains, the strength of the ice is mostly dominant in the mechanical behavior of the soil (Andersland et al., 2003).

The current study was presumably based on the remodeled soil condition, as it was not possible to quantify and achieve the undisturbed state of the frozen soil, therefore the methods used. Even though the desired water saturation of the soil was obtained in the laboratory conditions, the situ ice/water saturation is distributed more complicated within the arrays of veins and soil matrix (Savigny and Morgenstern, 1986).

In terms of adfreeze strength, the results of this study led to the conclusion that the peak of the short-term strength is achieved shortly after applying the considered load. Respectively, a lower temperature of the frozen soil leads to a higher bonding between the soil-concrete surface. Presumably, for the CIP concrete piles because of a larger ice formation due to the temperature-dependent hydration process, the adfreeze strength appears to be slightly higher.

Even though the surface of the concrete cylinders is smoother than the CIP concrete piles, the results of the study were less representative for the smooth pile-soil bonding literature. Moreover, as has been mentioned, a similar-parameter study showed that the thawed zone that could be created around the pile-soil interface may increase the roughness of the pile (Weaver, 1979). This constitutes a slightly positive parameter for the soil-concrete interaction, as the ice matrix will manifest a higher grip within the soil-ice behavior of both materials.

For the bond-healing recovery strength, a clear bond mechanism was observed. Probably with time and under specific load conditions the results would be of a more value. However, the roughness of the soil after both stages and the higher bond between the soil-ice-concrete layers has been observed as an indicator for a higher bond healing recovery, as observed for the sample 4 in the second stage of testing.

The limitations of the tests could have been created an exaggeration in the response mechanism, as has been observed for the Stage 1 results. The temperature deviations in the Knekkis laboratory, and cold storage laboratory showed an increase adfreeze bonding, as compared to the existing literature. Therefore, creep shear tests could be considered of a rare interest for the current temperature fluctuations of up to 10˚C. Furthermore, the lack of proper methodology, or materials such as the steel support that had a distribution area of the force smaller than the area of the concrete cylinder, has to be considered when one is analyzing the results. Although the current study implied only the sort-term tests, the results could be of an interest for the pile design in the frozen soil.

5.2. Concrete cast-in-place behavior

Thermal measurements constituted an important step towards observing the post-cast behavior of the concrete samples. Comparison of the results with the simulations showed that the desired maturity can be achieved within the long-term period, as compared to the 20°C reference concrete.

Different observations have been encountered with the thermocouple and thermistor sensors. The principle of work is slightly differing, calibration drift can happen for the thermocouples and the accuracy of the thermistor is considered to be higher. However, thermistors also manifest a degree of error due to circuitry, materials and the model, thermal coupling, temperature conversion, and aging of the electronics and sensor(Noetzli et al., 2021).

Maturity function of the concrete depends merely on the temperature sensitivity of initial strength development (Carino and Lew, 2001). With a difference in the variables that we have, the maturity function differs from one sample of concrete to the other. Furthermore, heat of hydration did not have the same potential for both measurements (No.1 and No.2), that could be attributed to the measurement inaccuracy and/or a slightly different concrete mixture and permafrost temperature or water infiltrations.

Significance of the simulation is showed in the equivalent maturity age and compressive strength calculus over the time period, even though the simulation results may differ from reality due to the variables described in the results section. Achieving a certain degree of strength and maturity over a short period of 7 days represents an important feature for the local engineering practices.

In regard to the adfreeze shear forces, I consider that there is no need in a relatively high maturity or achieved compression strength as the piles are mainly adfreeze force related. If there is a lower temperature in the permafrost, in terms of strength and stability, the CIP structure positioned in the soil that counts on the adfreeze strength manifests a certain degree of reliability. Even though the maturity is not achieved completely, the adfreeze response is comparatively promising (as seen in the stage 2 sample 4). The main infrastructure problems could arrive only when the temperature of the permafrost, or perhaps the temperature of the pile itself due to conduction of the above heat, will become high enough that it will lead to the permafrost or soil-concrete layer thawing. At this point, the rates of settlement of the discussed pile will be considerably higher as for the piles that were completely cured and achieved a higher maturity degree. This effect could be due to more surface water and ice on top of the less mature concrete pile that had a higher rate of freezing, as seen in behavior of the sample 4. Therefore, the post-cast behavior of the CIP piles seems to show favorable results, as long as temperatures of the permafrost will continue to assure the freezing condition.

Another relevant aspect that should be pointed is that for the driven piles, during the driving process, most of the adfreeze bond in lost, and the remaining residual strength is attributed to the residual friction that depends substantially on the unknown normal pressure against the pile shaft, due to the mechanisms such as: slurry refreezing around the pile surface, direct driving of the pile in the frozen ground, or relatively undersized well (Ladanyi and Theriault, 2008). This is to point that the lateral pressure should not be reliable for the designing process as it will be lost up to 99% in 1 day, but should,

however, be considered when one is evaluating the results of pile loading stress in the permafrost (Ladanyi and Theriault, 2008).

Chapter 6: Conclusion

The measurements and tests performed in this study have directed to some answers for the questions that were asked in the beginning considering the curing of the cement slurry and adfeeeze bond strength behavior.

Relatively high adfreeze strength was obtained for the less mature samples, and in regard to that it was observed that the maturity of the concrete has a particular influence on the adfreeze bonding between the soil-concrete interface.

Many ice-concrete and soil-concrete bond adfreeze tests have been done up until now. Due to different objectives of the studies, variables, and absence of standardization or proper normative for the test methods, the results appear to be relatively hard to compare, presumedly (Barker et al., 2021).

Tests could be done with different concrete proportions, different curing temperatures, salinities, and different soil water content that can be easily controlled in lab conditions, but that was not possible. The degree of influence of salt, that is also impacting the adfreeze bond strength, may be determined consequently.

Speaking about the long-term adfreeze strength, the extrapolation with the short-term data, still has to be questionable, due to different influencing variables, as has been mentioned (Ladanyi and Theriault, 2008). Moreover, as it was pointed, the adfreeze residual healing is favorized by relatively high normal pressures and unfrozen water content in the soil. For the last part, considering the silty clayey soils that are dominant in the Longyearbyen area, the recovery process of the strength may be more pronounced as for the frozen sandy soils, for example.

The incapacity of achieving the undisturbed soil conditions is another issue that was observed. As has been stated, since cryogenic textures of the ground ice and stratified ice cannot be recovered in artificial samples, it is desirable to also perform tests on the natural undisturbed permafrost (Savigny and Morgenstern, 1986).

Arctic infrastructure design, and merely the critical operations should not be solely dependent on the maturity age or the strength-maturity relationships, due to a higher sensitivity of the environment and, moreover, the need in a precise verification of the strength parameters for the cast-in-place concrete (Carino and Lew, 2001).

Eventually, the current analysis provided answers to some of the raised problems. Further studies and research have to be done, in order to extrapolate and observe the behavior of the cast-in-place concrete piles in the frozen soil, by taking into the account the effects of different temperatures of the permafrost, unfrozen water content or ice saturation, salinity, and the long-term creep of the shear adfreeze strength. Giving the advice of an increase in the instrumentation for the local laboratories, the methodology and standardization of the procedures must be assessed, consequently, in order to obtain a higher reliability of the tests. Finally, other sustainable alternatives for the slurry material could be analyzed, such as silt-clay or silt-sand slurry.

Bibliography

Andersland, O.B., Ladanyi, B., ASCE, 2003. Frozen Ground Engineering, 2nd Edition. Wiley.

Arenson, L.U., Springman, S.M., Sego, D., 2006. The rheology of frozen soils. Appl. Rheol. 17.

Ballim, Y., Graham, P.C., 2004. A numerical model for predicting time-temperature profiles in concrete structures due to the heat of hydration of cementitious materials.

Ballim, Y., Graham, P.C., 2003. A maturity approach to the rate of heat evolution in concrete. Mag. Concr. Res. 55, 249–256. https://doi.org/10.1680/macr.2003.55.3.249

Bårdseth, A., 2020. This is how the new school can be [WWW Document]. SVALBARDPOSTEN. URL https://www.svalbardposten.no/byggesaker-sjoskrenten-store-norske/slik-kan-den-nye-skolen-bli/201592 (accessed 7.2.22).

Barker, C.A., Bruneau, S., Colbourne, B., 2021. Adhesion of Ice to Concrete: Studies and Standardization.

Barker, J., Thomas, H., 2013. Geotechnical engineering in cold regions. ISCORD 2013 Plan. Sustain. Cold Reg. - Proc. 10th Int. Symp. Cold Reg. Dev. 204–214. https://doi.org/10.1061/9780784412978.020

Brouchkov, A., 2002. Nature and distribution of frozen saline sediments on the Russian Arctic coast. Permafr. Periglac. Process. 13, 83–90.

Budhu, M., 2010. Soil Mechanics and Foundations, 3rd Edition. ed. University of Arizona, Tucson.

Byggebransje, N., 2021. Hæhre is building a new folk high school in Longyearbyen [WWW Document]. Nor. Byggebransje. URL https://norskbyggebransje.no/nyheter/haehre-bygger-folkehogskole-i-longyearbyen (accessed 7.2.22).

Campbell, S., n.d. CR1000X: Measurement and Control Datalogger [WWW Document]. URL https://www.campbellsci.com/cr1000x#documents_ (accessed 7.3.22).

Carino, N.J., Lew, H.S., 2001. THE MATURITY METHOD: FROM THEORY TO APPLICATION. Gaithersburg, MD 20899-8611 USA.

Eranti, E., Lee, G.C., 1983. Introduction to Cold regions Structural Design and Construction. Buffalo.

Fredvik, T., n.d. HETT ’97 | Norcem AS in Norway [WWW Document]. URL https://www.norcem.no/no/Herdeteknologi (accessed 7.4.22).

Gilbert, G.L., Instanes, A., Sinitsyn, A.O., Aalberg, A., 2019. Characterization of two sites for geotechnical testing in permafrost: Longyearbyen, Svalbard. AIMS Geosci. 5, 868–885. https://doi.org/10.3934/geosci.2019.4.868

Gilbert, G.L., O’Neill, H.B., Nemec, W., Thiel, C., Christiansen, H.H., Buylaert, J.P., 2018. Late Quaternary sedimentation and permafrost development in a Svalbard fjord-valley, Norwegian high Arctic. Sedimentology 65, 2531–2558. https://doi.org/10.1111/SED.12476

Gold, L.W., 1970. Process of failure in ice. Can. Geotech. J. 7, 405–413. https://doi.org/10.1139/T70-052

Hansbo, S., 1958. A NEW APPROACH TO THE DETERMINATION OF THE SHEAR STRENGTH OF CLAY BY THE FALL-CONE TEST. R. SWEDISH Geotech. Inst. PROCEEDINGS No.14.

Heginbottom, J., Brown, J., Ferrians, O., Melnikos, E.S., 2002. Circum-Arctic Map of Permafrost and Ground-Ice Conditions, Version 2. Colorado, USA.

Hou, X., Chen, J., Yang, B., Wang, J., Dong, T., Rui, P., Mei, Q., 2022. Monitoring and simulation of the thermal behavior of cast-in-place pile group foundations in

permafrost regions. Cold Reg. Sci. Technol. 196, 103486. https://doi.org/10.1016/J.COLDREGIONS.2022.103486
Instanes, A., 2002. Climate change and possible impact on Arctic infrastructure. Phillips al. 1, 461–466.
ISO, I.O. for S., 2018. ISO 17892-12:2018(en), Geotechnical investigation and testing — Laboratory testing of soil — Part 12: Determination of liquid and plastic limits [WWW Document]. URL https://www.iso.org/obp/ui/#iso:std:iso:17892:-12:ed-1:v1:en (accessed 6.29.22).
ISO, I.O. for S., 2017. ISO 17892-6:2017(en), Geotechnical investigation and testing — Laboratory testing of soil — Part 6: Fall cone test [WWW Document]. URL https://www.iso.org/obp/ui/#iso:std:iso:17892:-6:ed-1:v1:en (accessed 6.29.22).
ISO, I.O. for S., 2016. ISO 17892-4:2016(en), Geotechnical investigation and testing — Laboratory testing of soil — Part 4: Determination of particle size distribution [WWW Document]. URL https://www.iso.org/obp/ui/#iso:std:iso:17892:-4:ed-1:v1:en (accessed 6.29.22).
Istanes, A., Anisimov, O., Brigham, L., Goering, D., Khrustalev, L.N., Ladanyi, B., Larsen, J.O., 2005. Infrastructure: Buildings, Support Systems, and Industrial Facilities, in: Arctic Climate Impact Assessment 38.
Istanes, A., L. Rongved, J., 2017. Forventede klimaendringers påvirkning på byggegrunn i Longyearbyen-området.
Istanes, A., Rongved, J.L., 2019. Climate change and geotechnical design in permafrost and frozen ground. XVII Eur. Conf. Soil Mech. Geotech. Eng. https://doi.org/10.32075/17ECSMGE-2019-0676
Jonassen, T., 2021. Building the World's Northernmost Folk High School in Svalbard [WWW Document]. HIGH NORTH NEWS. URL https://www.highnorthnews.com/en/building-worlds-northernmost-folk-high-school-svalbard (accessed 7.2.22).
Just Andersen, P., Elbaek Andersen, M., Whiting, D., 1992. A Guide to Evaluating Thermal Effects in Concrete Pavements. Washington.
Khalilzad, S., Sheshpari, M.M., 2016. A Review on Permafrost Geotechnics, Foundation Design And New Trends. Int. J. Res. Eng. Sci. 4, 59–71.
Ladanyi, B., Theriault, A., 2008. A STUDY OF SOME FACTORS AFFECTING THE ADFREEZE BOND OF PILES IN PERMAFROST. Cent. d'inginierie Nord. Ec. Polytech. Montr.
Ladanyi, B., Theriault, A., 1990. A study of some factors affecting the adfreeze bond of piles in permafrost. Int. Proc. Geotech. Eng. Cong. GSP 27 213–224.
Mehta, P.K., Monteiro, P.J.M., 2014. Concrete : microstructure, properties, and materials, Concrete: Microstructure, Properties, and Materials. McGraw-Hill Education.
Noetzli, J., Arenson, L.U., Bast, A., Beutel, J., Delaloye, R., Farinotti, D., Gruber, S., Gubler, H., Haeberli, W., Hasler, A., Hauck, C., Hiller, M., Hoelzle, M., Lambiel, C., Pellet, C., Springman, S.M., Vonder Muehll, D., Phillips, M., 2021. Best Practice for Measuring Permafrost Temperature in Boreholes Based on the Experience in the Swiss Alps. Front. Earth Sci. 9, 280. https://doi.org/10.3389/FEART.2021.607875/BIBTEX
Norwegian Polar Insitute, n.d. TopoSvalbard - Norsk Polarinstitutt [WWW Document]. URL https://toposvalbard.npolar.no/ (accessed 12.8.21).
NPRA, N.P.R.A., 1996. Hardener control - temperature measurement and firmness determination [WWW Document]. Statens Vegv. URL https://www.vegvesen.no/s/vegnormaler/hb/014/Gamle_filer/14.65/014-654.pdf (accessed 7.3.22).
Parameswaran, V.R., 1980. Adfreeze strength of frozen sand to model piles. Int. J. Rock Mech. Min. Sci. Geomech. Abstr. 17, 53. https://doi.org/10.1016/0148-9062(80)91567-3
Ranjan, G., Rao, A.S.R., 2007. Basic and Applied Soil Mechanics, 2nd Editio. ed. New Age International Publisher, New Delhi, India.
Rasmussen, T.H., Andersen, T., Oplysningskontor, C.T., CtO, 1989. Beton-teknik. Hærdeteknologig af beton.
Rubensdotter, L., 2015. LANDSKAPSFORMER OG LØSMASSER Bjørndalen-Vestpynten,

Svalbard.
Rubensdotter, L., n.d. Preliminary map, Landforms and Sediments, Longyearbyen valley.
Savigny, K.W., Morgenstern, N.R., 1986. Creep behaviour of undisturbed clay permafrost. Can. Geotech. J. 23, 515–527. https://doi.org/10.1139/T86-081
Sedaghat, A., 2016. Heat of Hydration and Thermal Control. University of South Florida.
Vyalov, S.S., 1963. Rheology of frozen soil. Publication 1287.
Wang, C., Dilger, W.H., 1994. Prediction of temperature distribution in hardening concrete. Therm. Crack. Concr. Early Ages 21–28.
Wang, K., Ge, Z., Grove, J., Mauricio Ruiz, J., Rasmussen, R., 2006. Developing a Simple and Rapid Test for Monitoring the Heat Evolution of Concrete Mixtures for Both Laboratory and Field Applications .
Weaver, J.S., 1979. Pile foundations in permafrost. The University of Alberta, Edmonton, Alberta. https://doi.org/10.7939/R3RX93Q02
Weaver, J S, Morgenstern, N.R., 1981. PILE DESIGN IN PERMAFROST. Can. Geotech. J. 18, 357–370.
Weaver, J. S., Morgenstern, N.R., 1981. Simple shear creep tests on frozen soils. Can. Geotech. J. 18, 217–229. https://doi.org/10.1139/T81-026

A. Appendices

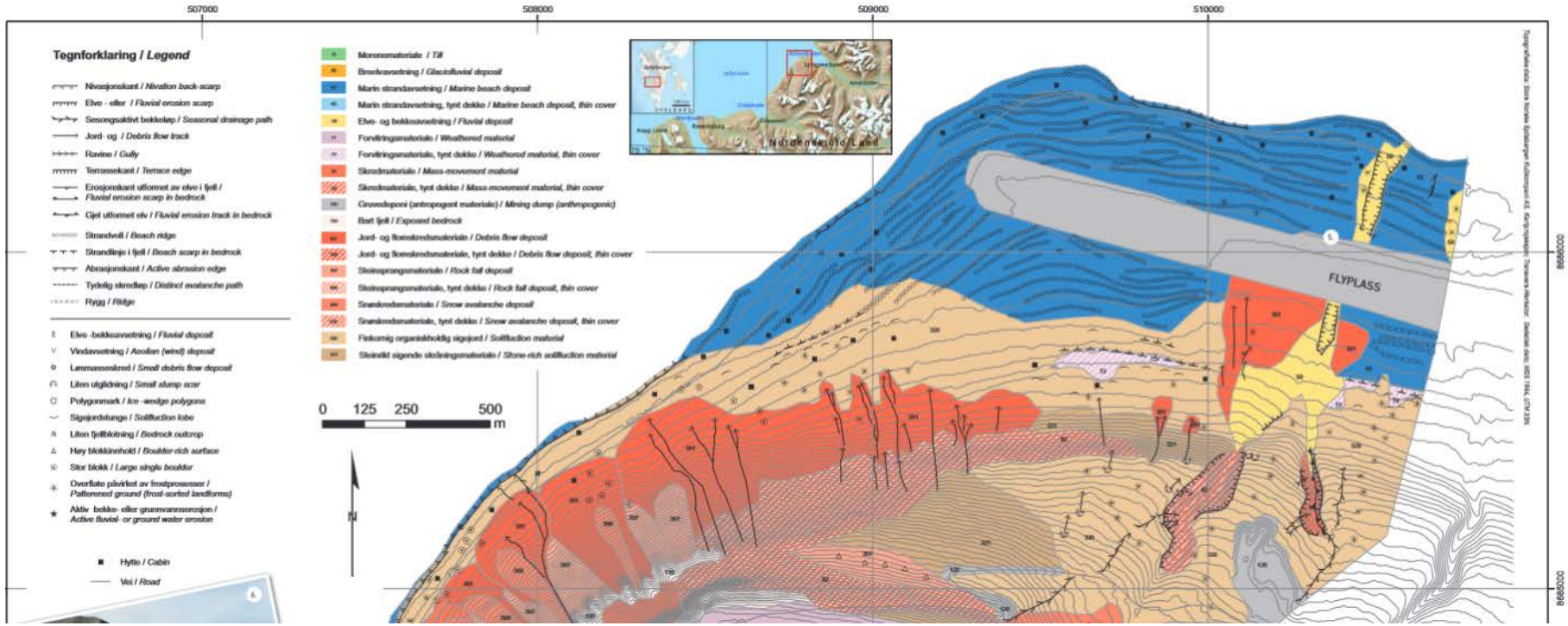

Figure A.1 Topsoil map of Bjørndalen-Vestpynten (Rubensdotter, 2015)

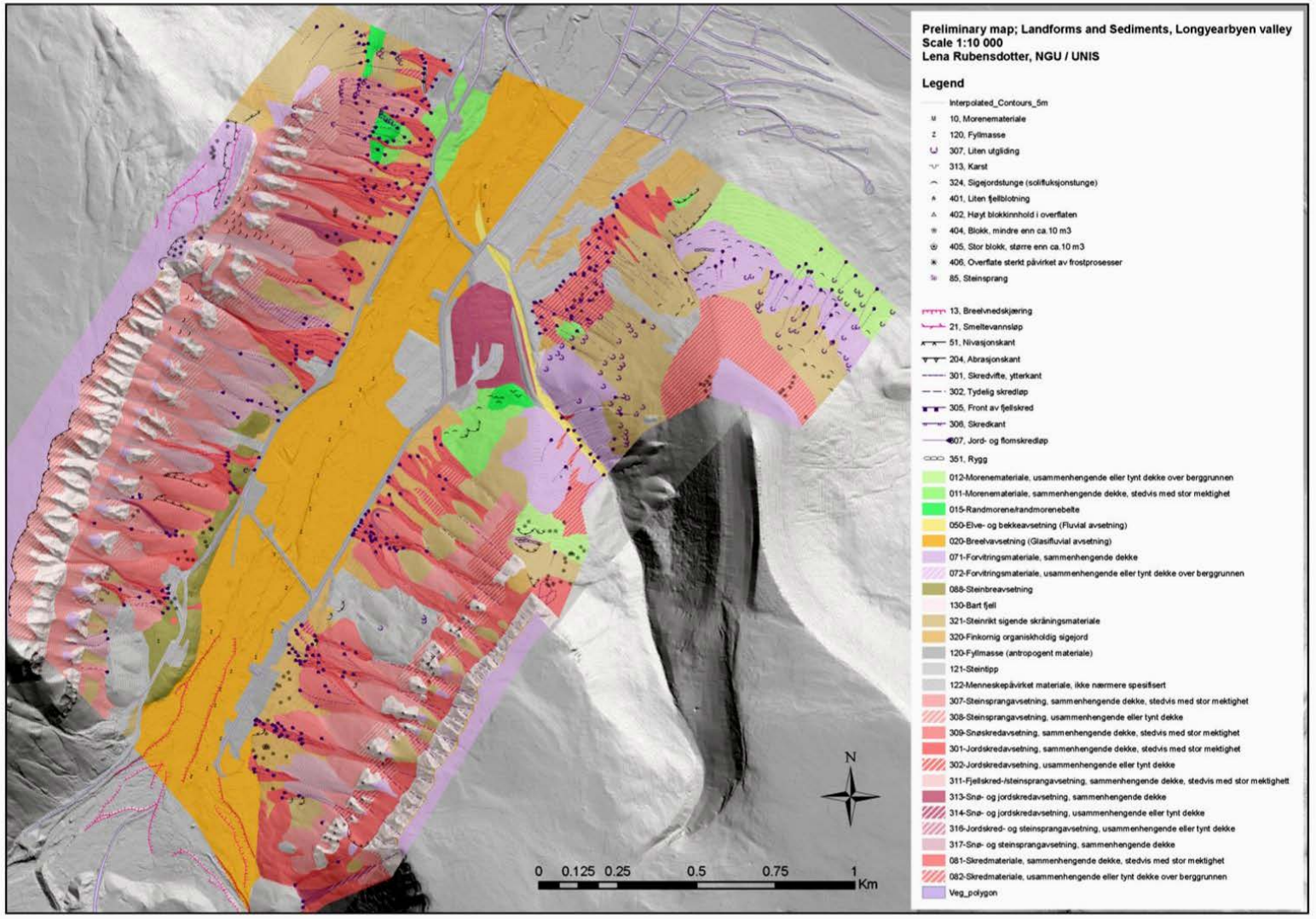

Figure A.2. Topsoil map of Longyeardalen (Rubensdotter, n.d.)

Figure A.3 UNIS East – Multiconsult drilling

Figure A.4. Drone image from the North direction - Pile installation and the existing infrastructure is visible (picture belongs to Hæhre Arctic).

Figure A.5. Image shows the drilling machine (left) and driven pile with the crawler excavator by use of a grapple claw (right)

Figure A.6. Thermocouples installation 16/02/2022: (a) – showing the depth below the ground, and (b) – showing the logger (yellow) and 2 green channels going on along the pile length

B30 - M60 FINSATS V/C 0,53												
	m3	m3	m3	m3	m3	m3	m3	m3	m3	m3	m3	
	1,0	1,5	2,0	2,5	3,0	3,5	4,0	4,5	5,0	5,5	6,0	
Sement	390	585	780	975	1170	1365	1560	1755	1950	2145	2340	Kg
Sand 0-8mm	1720	2580	3440	4300	5160	6020	6880	7740	8600	9460	10320	Kg
Pukk 8-16mm	0	0	0	0	0	0	0	0	0	0	0	Kg
Vann	206	309	412	515	618	721	824	927	1030	1133	1236	Liter
SX-N	4	6	8	10	12	14	16	18	20	22	24	Liter

3% fukt

B30 - M60 FINSATS V/C 0,53 med 3%fukt												
	m3	m3	m3	m3	m3	m3	m3	m3	m3	m3	m3	
	1,0	1,5	2,0	2,5	3,0	3,5	4,0	4,5	5,0	5,5	6,0	
Sement	390	585	780	975	1170	1365	1560	1755	1950	2145	2340	Kg
Sand 0-8mm	1771	2657	3542	4428	5313	6199	7084	7970	8855	9741	10626	Kg
Pukk 8-16mm	0	0	0	0	0	0	0	0	0	0	0	Kg
Vann	258	387	516	645	774	903	1032	1161	1290	1419	1548	Liter
SX-N	4	6	8	10	12	14	16	18	20	22	24	Liter

Figure A.7 Density of the concrete compounds (fukt = moisture)

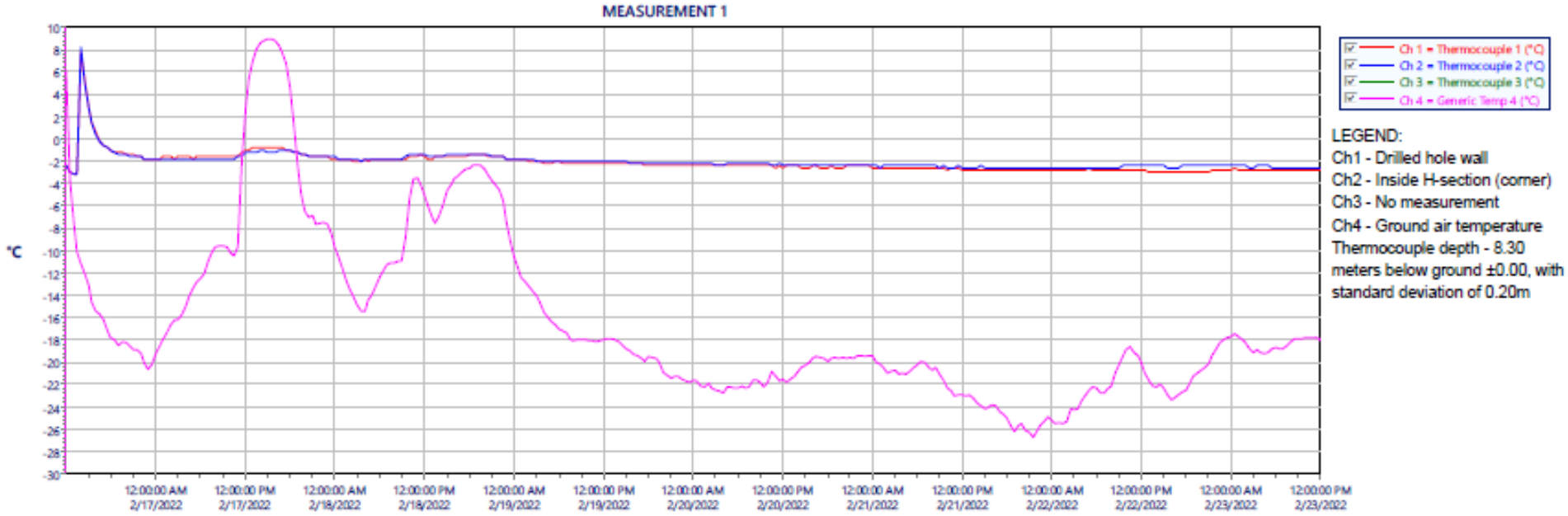

Figure A.8 Measurements 1 logging of a 7-day period

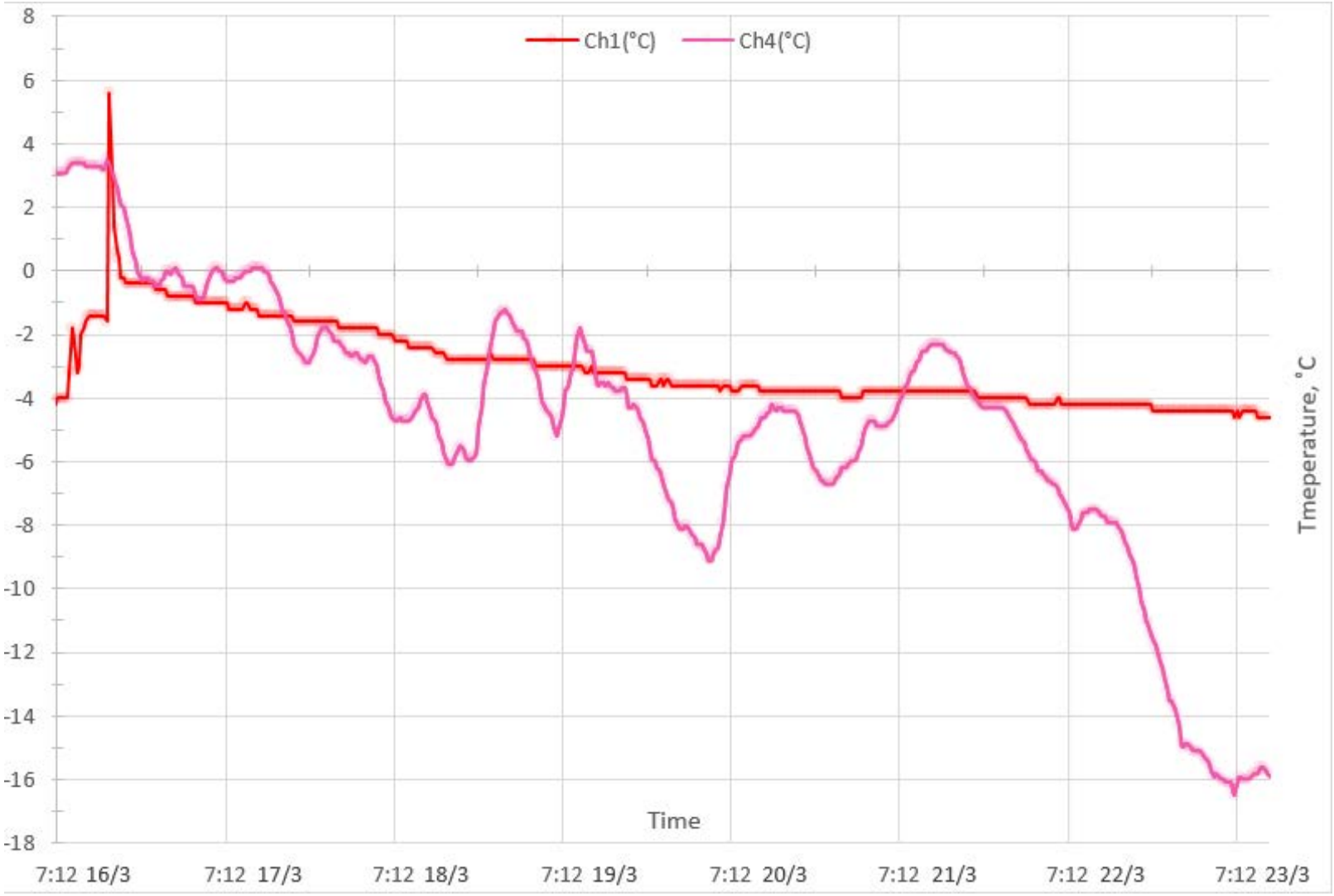

Figure A.9 Measurements 2 logging of a 7-day period

Figure A.10. Thermocouple and Thermistor installation after 16/03/2022: (a) – concrete pouring via the excavator cup on the analyzed pile located close to the existing building, and (b) – checking the setup of the thermocouple and thermistors.

Diligence Ev

Comark N2000 Series Data Loggers

Specifications

Sensor Type	
N2011, N2012, N2013	Thermistor
N2014	Type K or Type T thermocouple
Connector	Lumberg
Measurement Range	
N2011, N2012 internal sensor	-40°C to +70°C / -40°F to +158°F
N2012 external sensor	-40°C to +150°C / -40°F to +302°F
N2013 temperature	-20°C to +60°C / -4°F to +140°F
N2013 humidity	0 to 97% RH non condensing
N2014 - Type K	-200°C to +1372°C / -392°F to +2500°F
N2014 - Type T	-200°C to +400°C / -392°F to +752°F
N2014 - Thermistor	-40°C to +70°C / -40°F to +158°F
N2015	4 to 20mA
Scales	
Temperature	°C and °F
Humidity	RH or DP
Displayed Resolution	
Temperature	0.1° (1° below -100°C, -148°F and above +1000°C or °F)
Humidity	0.1% RH
N2014	0.2*
N2015 only	4 digits 1 decimal place (software allows 0 to 4 decimals in logged data)
Internal Accuracy at +20°C/+65°F ambient	
N2014	±0.5°C +0.5% (±0.9°F +0.5%) of reading over the range of -80°C to thermocouple limit
N2015	±0.3% of full scale
Memory	32K
1 channel	16000 samples
2 channels	8000 samples
3 channels	5300 samples
4 channels	4000 samples
5 channels	3200 samples
Logging Frequency	Programmable between 1 second and 99 hours,
N2014	2 seconds to 99 hours
Communications	Via infrared interface
Download Time	3 minutes per 10,000 readings (typical)
Ambient Storage	-40°C to +70°C/-40°F to +158°F
Battery Type	1 x AA size 3.6V replaceable lithium battery
Case Material	ABS
Environmental Protection	IP67, EN 60529, IEC 529

For more details fo the Diligence WIFI range, please see www.comarkinstruments.com

* Software selection of decimals will affect recorded values, e.g. selection of 0 decimals = 1 value of ±32000 and a selection of 4 decimals = a value of ±3.2000

Figure A.11 Data logger specification – N2014 Type K

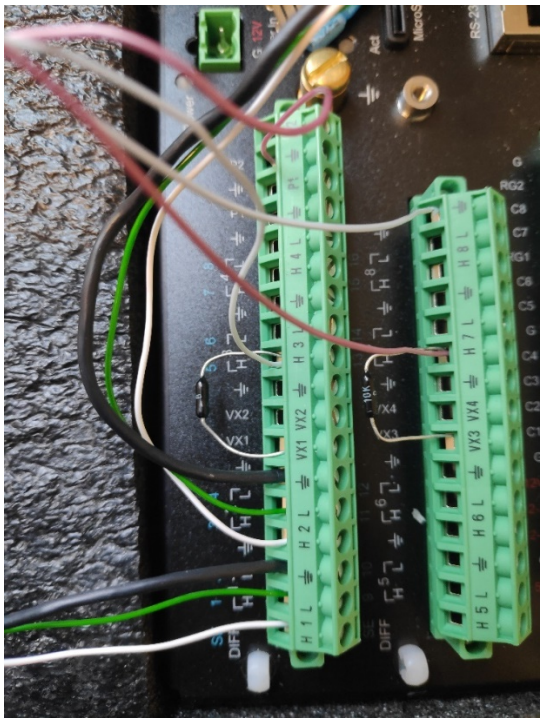

Figure A.12 Example of Campbell CR1000X wiring setup: 2 heat plates (left corner down) and 2 thermistors connected (top left and right)

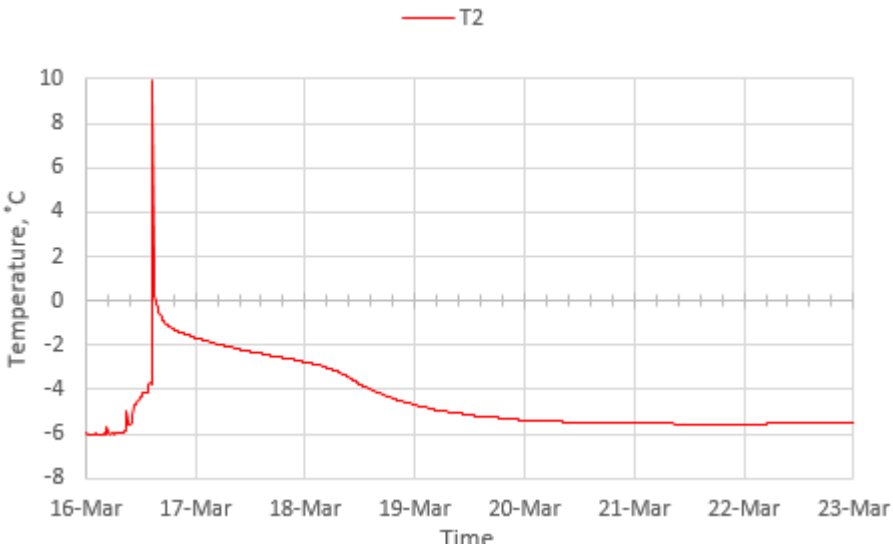

Figure A.13 Thermistor temperature data logging for the 7 days of logging

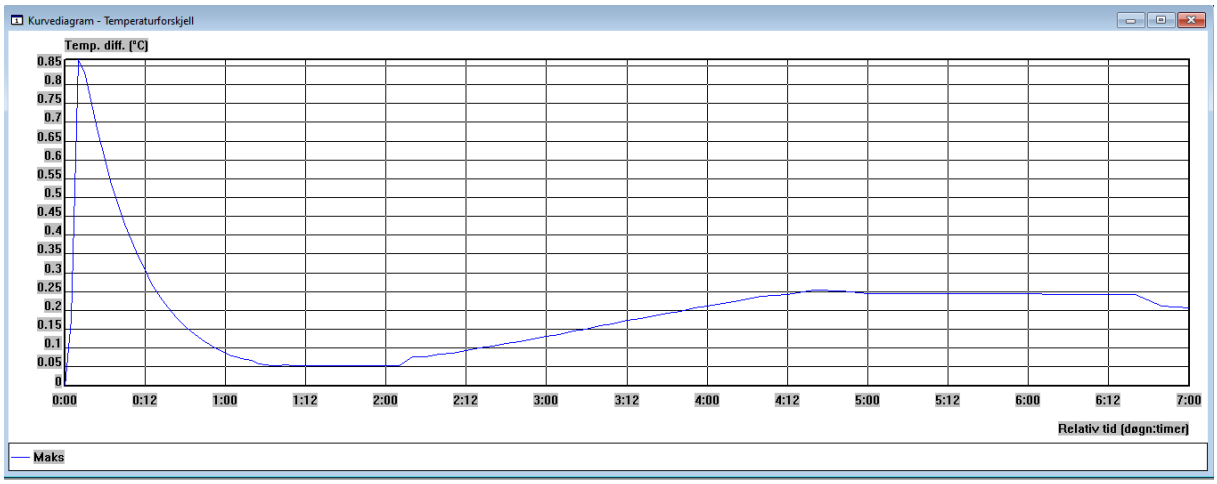

Figure A.14 Temperature difference in the concrete section (outer vs inner section)

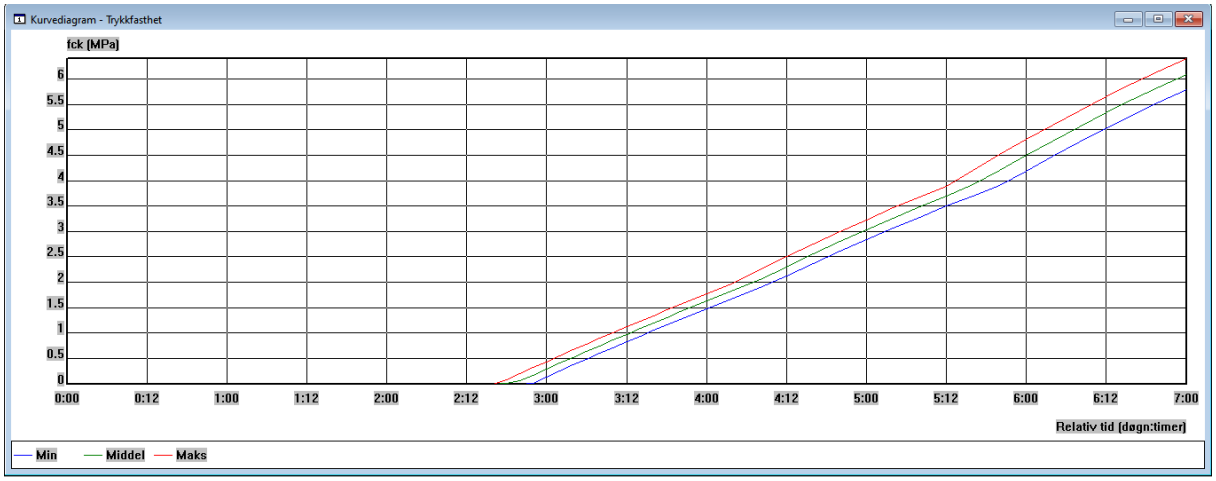

Figure A.15 Compressive strength development 7 days

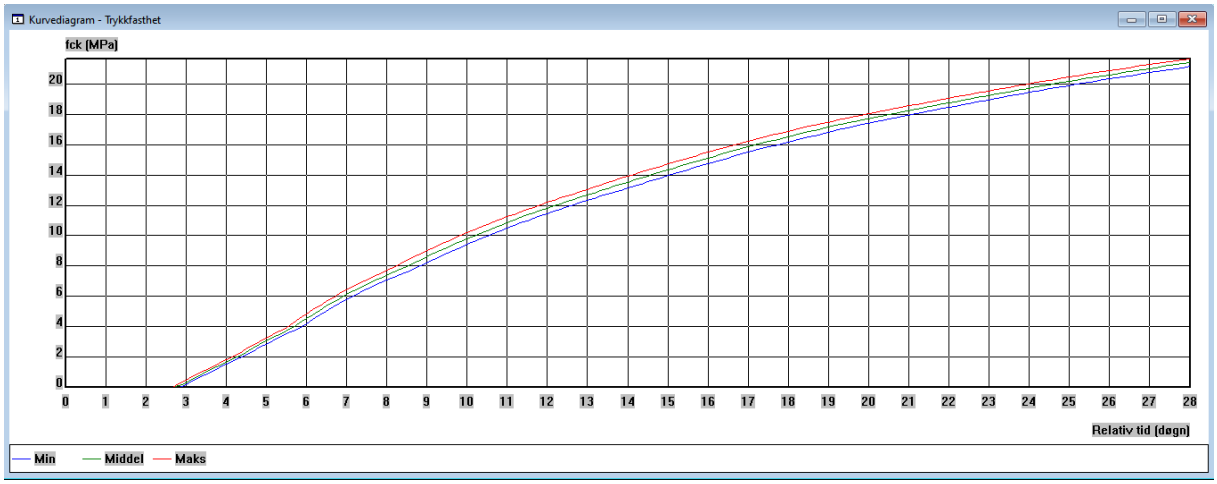

Figure A.16 Compressive strength development 28 days

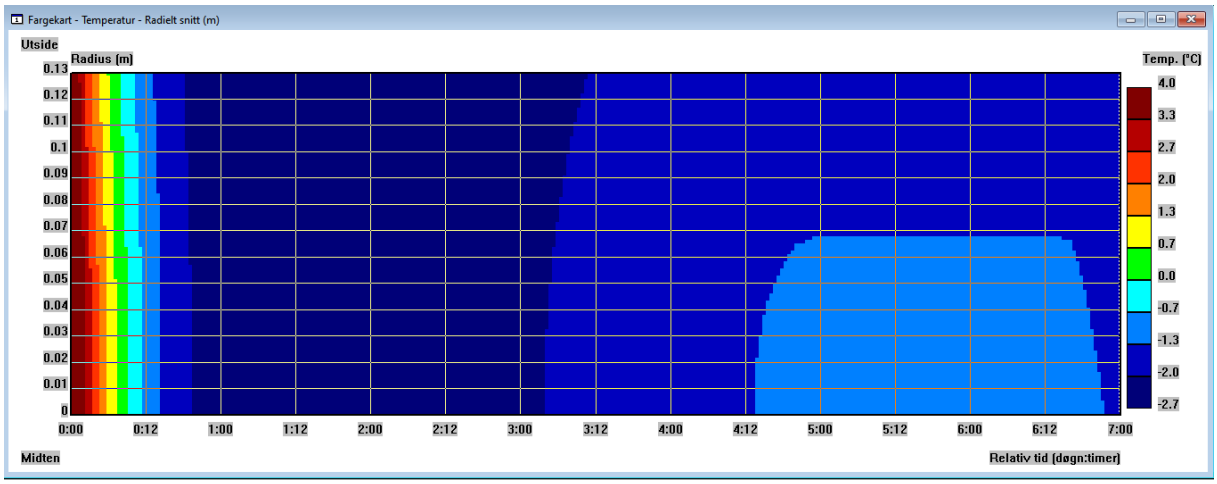

Figure A.17 Temperature distribution colored chart

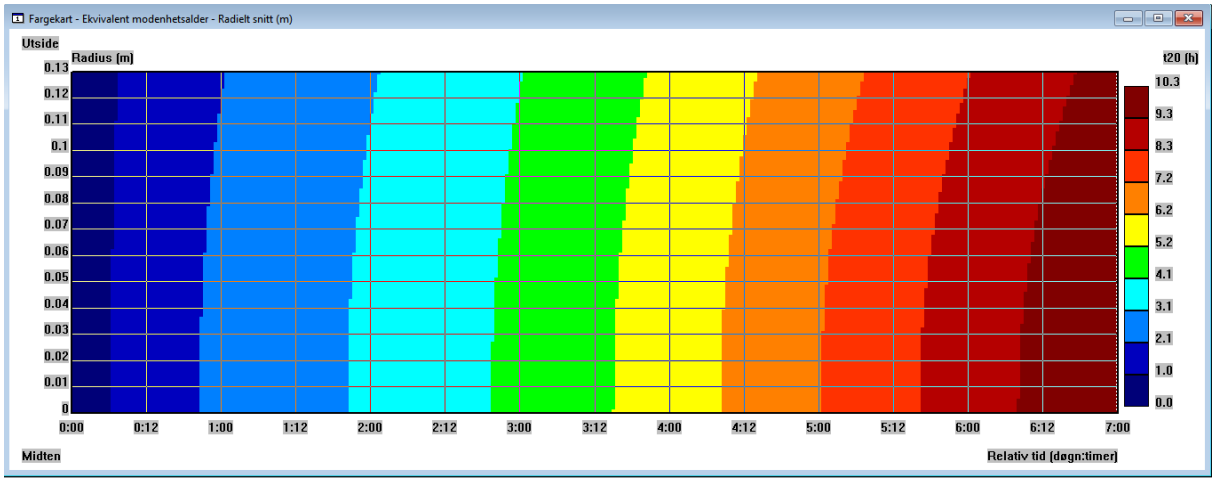

Figure A.18 Equivalent maturity age colored char

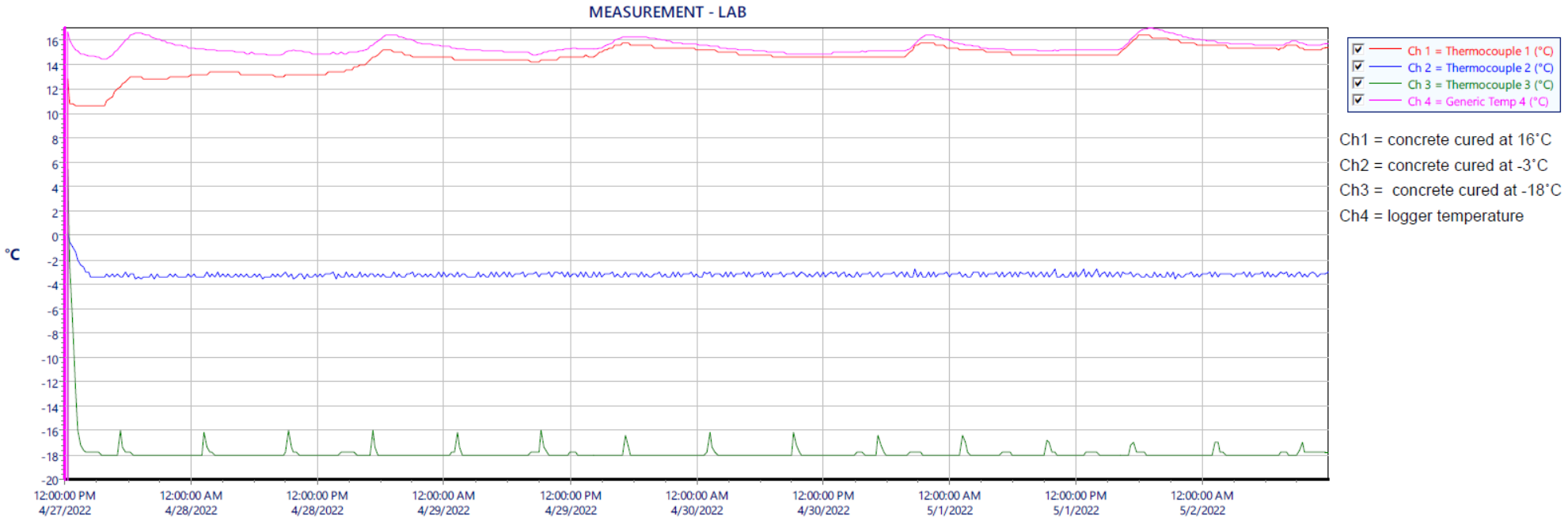

Figure A.19 Ten days temperature development of the lab-tested concrete

Figure A.20 Preparation of the concrete samples: middle – concrete cylinders and most right samples - thermally measured with the thermocouples.

Figure A.21 Preparation of the soil samples. left (a) - sample#1 preparation and right (b) - the four soil buckets isolated and located in the cold lab

Figure A.22 left (a) - Knekkis uniaxial compression machine and right (b) - a representative figure of the setup and the measured temperature

Figure A.23 Failure mechanism of stage 1 #1 sample: left (a) – adfreeze shear along the soil well, and right (b) – concrete cylinder out of the designed bucket hole

Figure A.24 Concrete samples after 2 stages of adfreeze shear tests, washed. From left to right sample #1 to #4.

Figure A.25 Stage 2 – sample #4 observation

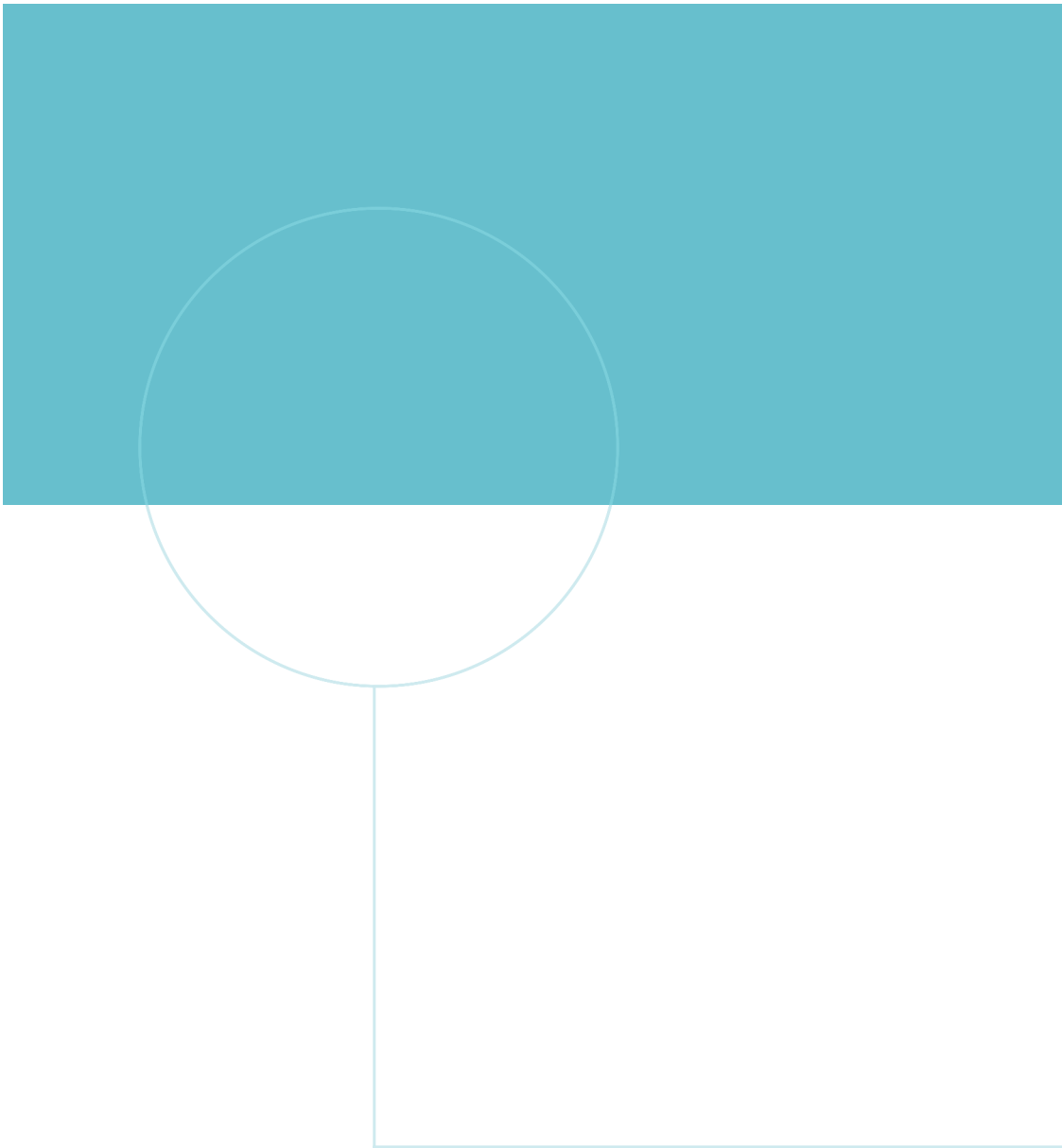

NTNU

Norwegian University of
Science and Technology